double-stranded cDNAs and hybridization to a GeneChip Mouse Genome 430 2.0 Array (Affymetrix), and the subsequent washing, staining and data analysis have been described previously (Kanno et al., 2006). All of these data are also now available online at the National Institute of Health Sciences (http://www.nihs.go.jp/tox/TtgSubmitted.htm).

Identification of the *Ripply2* somite enhancer

Highly conserved *Ripply2* upstream regions were identified using a cross-species DNA sequence comparison using the PipMaker website (http://pipmaker.bx.psu.edu/pipmaker/). We cloned a 5′ upstream genomic sequence of *Ripply2* from a bacterial artificial clone (RP23) contained in a mouse genomic library. A 1.5 kb DNA fragment containing the 171 bp highly conserved region was isolated by *Eco*RI and *Bam*HI digestion and then subcloned into the hsp-nlacZ reporter construct. Fertilized eggs from B6C3F1 female mice were collected for pronuclear injection and the injected eggs were then implanted into ICR female mice. Foster mothers were sacrificed at E10.5 and stained for β-galactosidase (β-gal) activity with X-Gal. The genotypes of the embryos were then identified by PCR using DNA prepared from the yolk sac.

Luciferase assay

For luciferase reporter analysis under the control of the 1.5 kb *Ripply2* anterior-PSM enhancer (*Eco*RI-*Bam*HI) fragment (20 ng), reporter constructs were co-transfected with the expression vectors 3xFLAG-Mesp2 (0, 30, 100 ng) and 3xFLAG-E47 (0, 50 ng) into NIH3T3 cells (0.25×10^5 cells per well in 24-multiwell plates) using Lipofectamine Plus (Invitrogen), following the manufacturer's instructions. The vector containing the *Renilla* luciferase gene under the control of the thymidine kinase promoter (1 ng) was co-transfected as an internal standard to normalize for transfection efficiency, and the amount of total plasmid was adjusted with pcDNA3.1. After 36 hours, luciferase activities were measured using a Dual Luciferase Assay Kit (Promega).

Electrophoretic mobility shift assay (EMSA)

A 3xFLAG-Mesp2 protein was produced using the FreeStyle 293 Expression System (Invitrogen) and then collected via a nuclear extraction method. Double-stranded DNA oligonucleotide probes were end-labeled with DIG and protein-DNA complexes were detected using a DIG Gel Shift Kit (Roche). Binding reactions were carried out for 30 minutes on ice, and protein-DNA complexes were analyzed on 6% native polyacrylamide gels.

Ripply2 gene targeting strategy

The mouse *Ripply2* gene consists of four exons, the first of which harbors two putative in-frame translational initiation codons. We generated a targeting vector with a floxed *neo* cassette to remove a portion of exon 1, which would introduce a termination codon just after the second initiation codon and produce a null allele. The resulting linearized vector (25 μg) was then electroporated into TT2 ES cells (Yagi et al., 1993). G418-resistant cell clones were further selected by PCR. Correct homologous recombination was confirmed by Southern blotting, and targeted cell clones were aggregated with ICR 8-cells and then transferred to pseudopregnant female recipients. The resulting chimeric mice were bred with ICR females. Germline transmission of the targeted allele was confirmed by PCR. The floxed neomycin cassette was later removed by breeding with a CAG-Cre transgenic mouse (Sakai and Miyazaki, 1997).

Gene expression and histochemical analysis

Methods for gene expression analysis by in situ hybridization of whole-mount samples and by skeletal staining have been described previously (Takahashi et al., 2000). The probes used in this study have been described previously (Takahashi et al., 2000; Takahashi et al., 2003; Nomura-Kitabayashi et al., 2002). For the *Ripply2* RNA probe, we used a full-length cDNA clone containing intron 1. Section in situ hybridization and immunohistochemical detection of proteins were performed as previously described (Morimoto et al., 2005). For whole-mount detection of Mesp2-venus, embryos were fixed with 4% paraformaldehyde in PBS overnight at 4°C, incubated with rabbit anti-GFP (MBL; 1:1000), followed by Alexa-488-conjugated goat anti-rabbit IgG (Molecular Probes; 1:400) and observed using a fluorescent microscope (Olympus BX61).

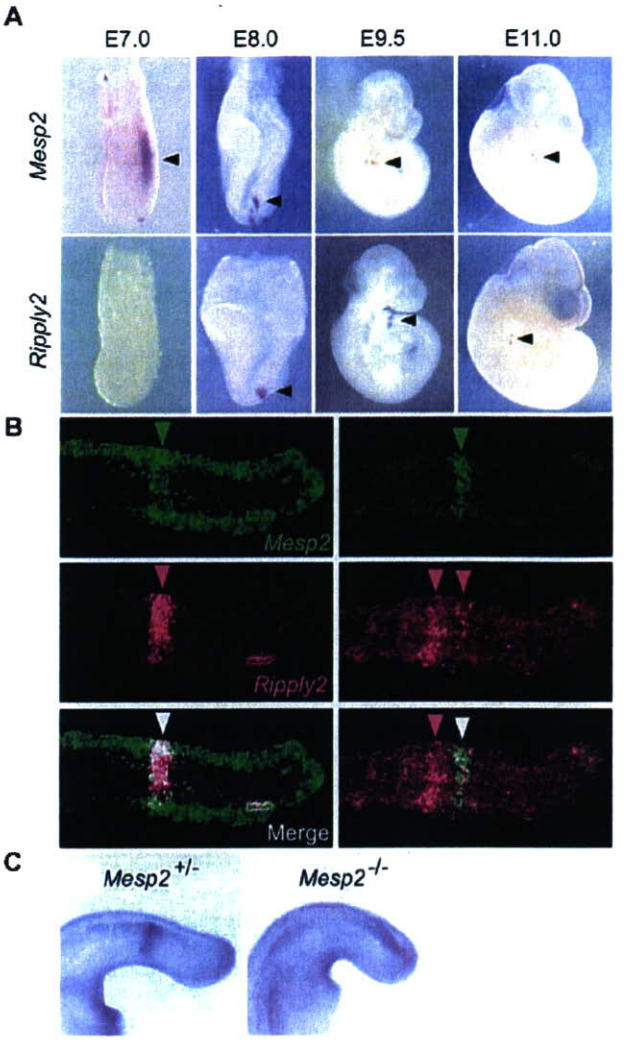

Fig. 1. Analysis of the of *Ripply2* expression pattern. (**A**) Comparison of the mRNA expression patterns of *Mesp2* and *Ripply2* during mouse development. Positive expression is indicated by an arrowhead. (**B**) Comparison of the spatial expression patterns of *Mesp2* and *Ripply2* as revealed by section double in situ hybridization. Two representative examples are shown for *Mesp2* (green) and *Ripply2* (magenta), and merged images of these expression patterns are shown beneath. The green signals in the periphery are artifacts and do not represent *Mesp2* expression. In some cases, only a single band could be observed for each gene, and these bands are merged in the image shown in the left-hand bottom panel. Two bands were sometimes visible for *Ripply2*, the posterior band of which merges with that of *Mesp2* (right-hand bottom panel). All samples were prepared from E10.5 embryos. (**C**) Whole-mount in situ hybridization showing that *Ripply2* expression is lost in the E9.5 *Mesp2*-null embryo.

RESULTS

Ripply2 is a possible direct target of Mesp2

Mesp2 is known to function as a transcriptional activator of genes, such as *Epha4* and *Lfng*, which are expressed in the rostral half of the presumptive somite (Morimoto et al., 2005; Nakajima et al., 2006). Moreover, expression of the *Dll1* and *Uncx4.1* genes, which are expressed in the caudal half of the somite (Bettenhausen et al.,

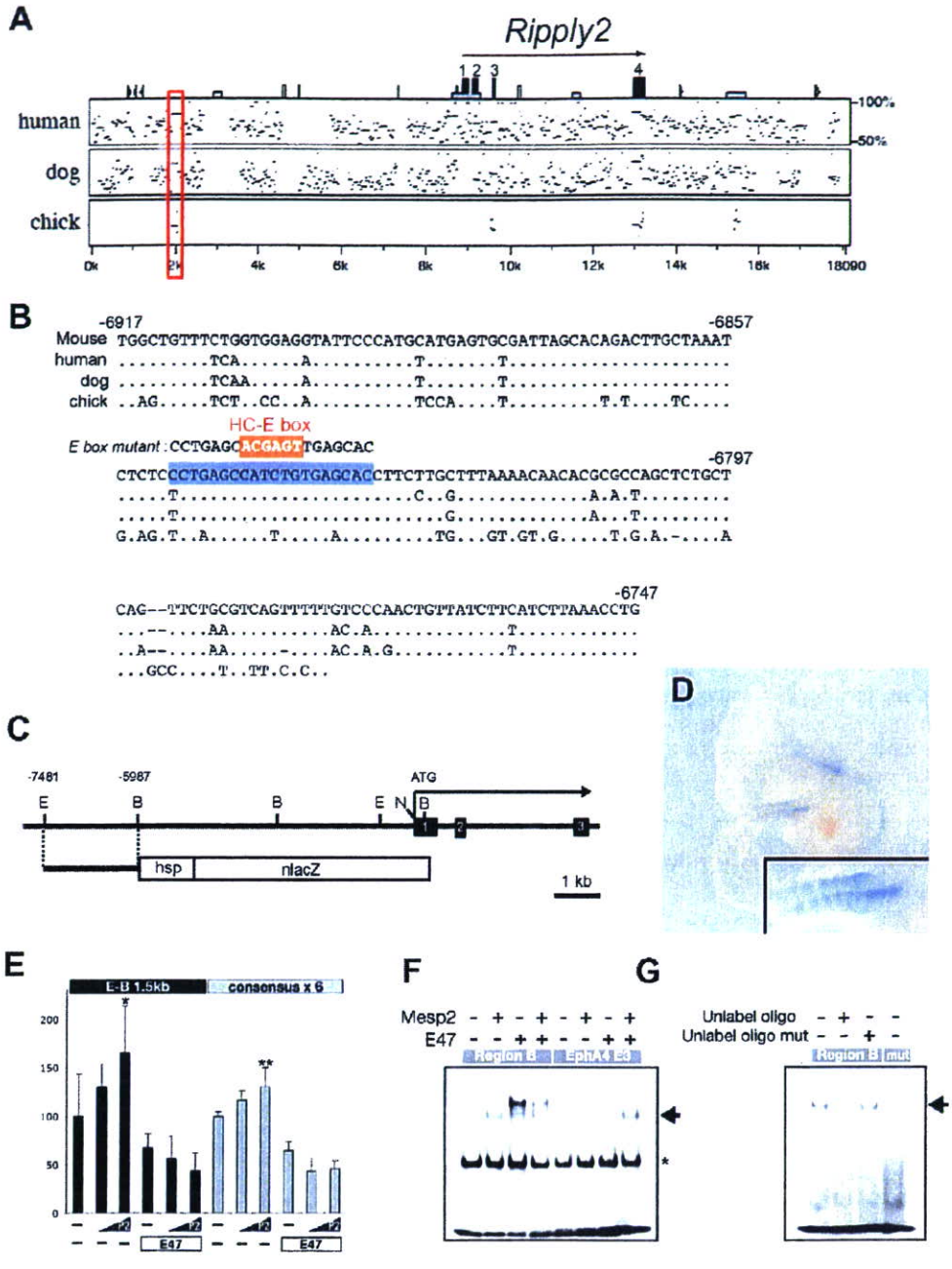

Fig. 2. Mesp2 can directly bind to the enhancer element of the *Ripply2* gene and activate its transcription. (**A**) Comparison of the genomic sequences around the *Ripply2* gene in mouse (top line) with those in human, dog and chick using MultiPipMaker sequence alignment software. A conserved region (framed in red) is evident across these species. (**B**) Sequence alignment of the 171 bp region conserved among the *Ripply2* genes, within which a highly conserved E-box is located. HC E-box, highly conserved E-box. (**C**) The genomic organization of the mouse *Ripply2* gene and the corresponding construct used in the transgenic analyses. A 1.5 kb DNA fragment containing this highly conserved 171 bp stretch (shown in A) of the *Ripply2* upstream region was ligated to a cassette composed of the *hsp* promoter and nlacZ (*lacZ* harboring a nuclear localization signal). E, *Eco*RI; B, *Bam*HI; N, *Nco*I. (**D**) The *Ripply2* enhancer drives *lacZ* reporter gene expression in somitic mesoderm cells at E11.0. The inset shows high magnification of the somitic region. (**E**) Luciferase reporter assay for *Mesp2* activation, with or without E47, using constructs harboring either the 1.5 kb *Ripply2* enhancer (left) or six repeats of the conserved 171 bp fragment (right). The addition of E47 had negative effects upon transactivation. The data represent the means±s.d. from four separate experiments. **P*<0.01, ***P*<0.04. (**F**) EMSA analyses revealing that a DNA fragment containing the conserved E-box (Region B, light-blue shading) from the *Ripply2* upstream region can bind Mesp2 in the absence of E47. This binding of Mesp2 thus appears to be different from its binding to the *Epha4* enhancer, which is dependant upon E47. Non-specific bands are indicated by the asterisk. (**G**) The binding specificity of Mesp2 was confirmed by successful competition with cold probe, but not with an E-box mutant probe (shown in B).

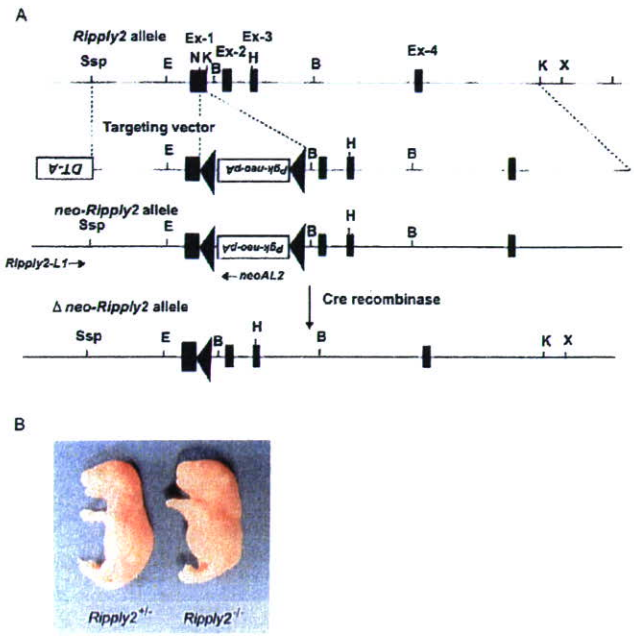

Fig. 3. The targeting strategy used for the *Ripply2* gene and the external morphology of the resulting knockout mouse. (**A**) The top line shows the genomic organization of the *Ripply2* gene, the second line represents the structure of the targeting vector, and the bottom two lines show the predicted structure of the *Ripply2* locus following homologous recombination. The first exon of *Ripply2* was partially deleted and replaced with a floxed *neo* cassette (the arrowheads on the line represent loxP sites). A germline chimeric mouse was then generated from recombinant ES cells containing the targeted allele and crossed with a CAG-Cre mouse to remove the *neo* cassette and establish the *Ripply2*-knockout mouse line. Ssp, *Ssp*I; E, *Eco*RI; B, *Bam*HI; H, *Hind*III; N, *Nco*I; K, *Kpn*I; X, *Xho*I. (**B**) The *Ripply2*-null mouse dies soon after birth and the external morphology at E17.5 is similar to those of segmentation-defective mutants, featuring a short trunk with rudimental tails.

1995; Leitges et al., 2000), is increased in the *Mesp2*-null mouse, indicating that Mesp2 is required for their suppression (Takahashi et al., 2000). However, the molecular mechanisms underlying this are unknown. To identify novel genes that operate downstream of Mesp2, we performed GeneChip analysis using RNAs prepared from both wild-type and *Mesp2*-null embryos. Among the genes that showed a reduction in expression in the *Mesp2*-null embryos (see Table S1 in the supplementary material), we selected a cDNA clone (corresponding to RIKEN cDNA C030002E08) that showed an identical expression pattern to that of *Mesp2* by in situ screening of 11.5 dpc embryos. This cDNA was subsequently revealed to be the mouse *Ripply2* gene recently reported by Kawamura et al. (Kawamura et al., 2005). The initial expression of *Mesp2* was found to be restricted to the nascent mesoderm at E7.0, but *Ripply2* expression appeared to be absent or very weak prior to somitogenesis (Fig. 1A). However, its expression became evident in the anterior PSM as a pair of bands by 8.0 dpc, similar to *Mesp2*

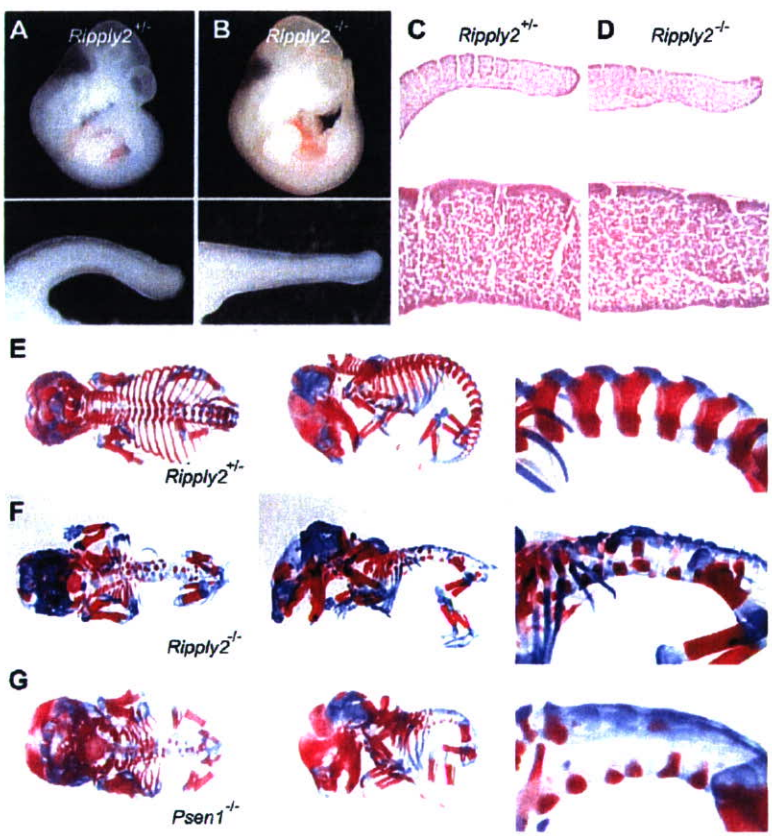

Fig. 4. The *Ripply2*-knockout mouse exhibits segmentation defects. (**A-D**) *Ripply2*$^{+/-}$ and *Ripply2*$^{-/-}$ embryos (n=3 at E10.5) were compared by external morphology (A,B) and by the Hematoxylin and Eosin staining of parasagittal sections of tail regions (C,D). *Ripply2*$^{-/-}$ embryos display irregularly sized myotomes, and an unclear segmental border. (**E-G**) Skeletal preparations at E17.5 stained with Alizarin Red-Alcian Blue reveal that the *Ripply2*$^{-/-}$ fetus harbors fewer pedicles of neural arches and lacks components of the proximal ribs (F; n=4), which is similar to the aberrant phenotype of the *Psen1*-null fetus (G; n=2).

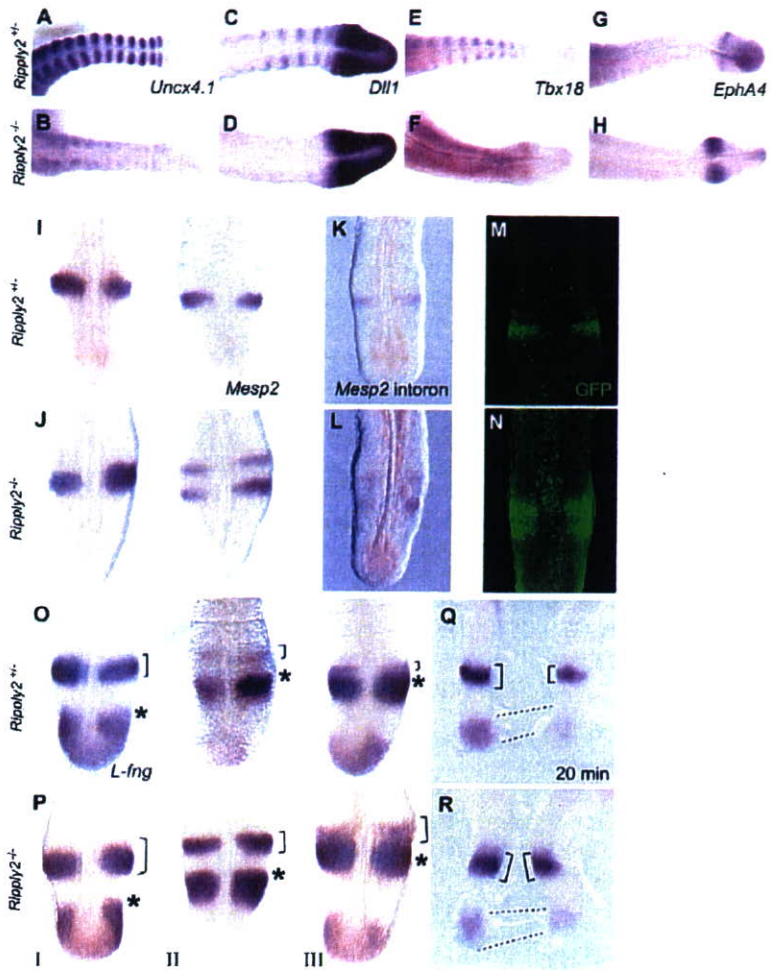

Fig. 5. Altered gene expression in the *Ripply2*-null embryos. Whole-mount in situ hybridizations were employed to characterize somitogenesis in the *Ripply2*$^{-/-}$ embryo. The expression of caudal genes such as *Uncx4.1* (**A**,**B**) and *Dll1* (**C**,**D**) was found to be reduced, whereas rostral genes such as *Tbx18* (**E**,**F**) and *Epha4* (**G**,**H**) show an expanded pattern in *Ripply2*$^{-/-}$ embryos at E11.5. (**I-N**) Comparisons of the expression patterns of *Mesp2* mRNA, detected by exon (I,J) and intron (K,L) probes, and protein levels (M,N), at E10.5. An additional *Mesp2* expression band appears rostrally in the *Ripply2*$^{-/-}$ embryos (J,L). Mesp2 protein expression, visualized by Mesp2-venus, was compared between the *Ripply2*$^{+/-}$ (M, *n*=2) and *Ripply2*$^{-/-}$ (N, *n*=3) genetic backgrounds. The confocal images were visualized by fluorescence, detected using anti-GFP antibodies. (**O**,**P**) Comparison of the *Lfng* expression patterns at different cyclic phases (indicated by I to III) at E10.5. The oscillatory expression of *Lfng* (asterisks) in the posterior PSM was unaffected, but the rostral-most expression bands (brackets) are slightly expanded in the *Ripply2*$^{-/-}$ embryos (P), as compared with the *Ripply2*$^{+/-}$ embryos (O). (**Q**,**R**) The prolonged expression of *Lfng* in the anterior PSM. The PSM of E10.5 *Ripply2*$^{+/-}$ (Q) and *Ripply2*$^{-/-}$ (R) embryos was separated into two halves, with one being fixed immediately and the other fixed after explant culturing for 20 minutes. Both were then analyzed for *Lfng* mRNA. The expression of *Lfng* in the anterior PSM is maintained for longer in the *Ripply2*$^{-/-}$ embryos.

(Fig. 1A). The expression of *Ripply2* then continued until 12.5 dpc, during the somite-forming period (Fig. 1A and data not shown). The expression domains of *Mesp2* and *Ripply2* were next compared by double in situ hybridization of embryonic tail sections. Two typical patterns are shown in Fig. 1B. One shows single bands that are completely merged, whereas the other is of a single *Mesp2* band and two *Ripply2* bands in which the caudal band is merged with a distinct *Mesp2* band. This observation indicates that *Mesp2* expression precedes that of *Ripply2*, but that *Ripply2* persists for longer. In addition, *Ripply2* expression was lost in the *Mesp2*-null embryo (Fig. 1C), as predicted from our GeneChip analysis. These data thus indicated that *Ripply2* might be a target of Mesp2.

To examine this possibility, we searched for possible cis-regulatory sequences in the *Ripply2* gene by comparing mouse, human, dog and chick genomic sequences using MultiPipMaker sequence alignment software (Fig. 2A). From these analyses, we identified a conserved region (–6917 to –6747, Fig. 2B). To investigate whether the 1.5 kb region containing this conserved 171 bp sequence (Fig. 2B) possessed enhancer activity, we performed transient transgenic analyses using a β-gal reporter (Fig. 2C). In five out of nine PCR-positive embryos, we detected specific β-gal expression in several segmented somites (Fig. 2D), which is a typical pattern for genes expressed in the anterior PSM, including *Mesp2* and *Epha4* (Haraguchi et al., 2001; Nakajima et al., 2006). We next employed a luciferase reporter assay system to ascertain whether the enhancer activity was dependant upon Mesp2. Two reporter constructs were generated – one containing the 1.5 kb genomic fragment and the other harboring six repeats of the 171 bp consensus sequence. Both constructs were activated by the addition of Mesp2, but not in conjunction with E47 (also known as Tcfe2a – Mouse Genome Informatics) (Fig. 2E). This result was different from the findings of our previous study of the *Epha4* enhancer (Nakajima et al., 2006), in which Mesp2 was observed to bind and transactivate the reporter activity only in the presence of E47, a possible heterodimeric partner. Since Mesp2 belongs to the bHLH-type transcription factor family, which is known to bind either to E-box or N-box motifs, we screened the 171 bp *Ripply2* gene consensus sequence for E-boxes, or for an N-box which is capable of binding to Mesp2 with or without E47. We identified a DNA fragment containing a highly conserved E-box CATCTG sequence, and confirmed that this binds to Mesp2, whereas a mutated form did not (Fig. 2F,G). E47 was also found to bind to this E-box, but this might not be functional binding as no associated activity was detectable by luciferase reporter assay. Furthermore, the binding of Mesp2 was weakened by the addition of E47. These results are consistent with the idea that Mesp2 binds to this E-box in the enhancer of the *Ripply2* gene, and that this enhancer does not require E47 for subsequent transactivation.

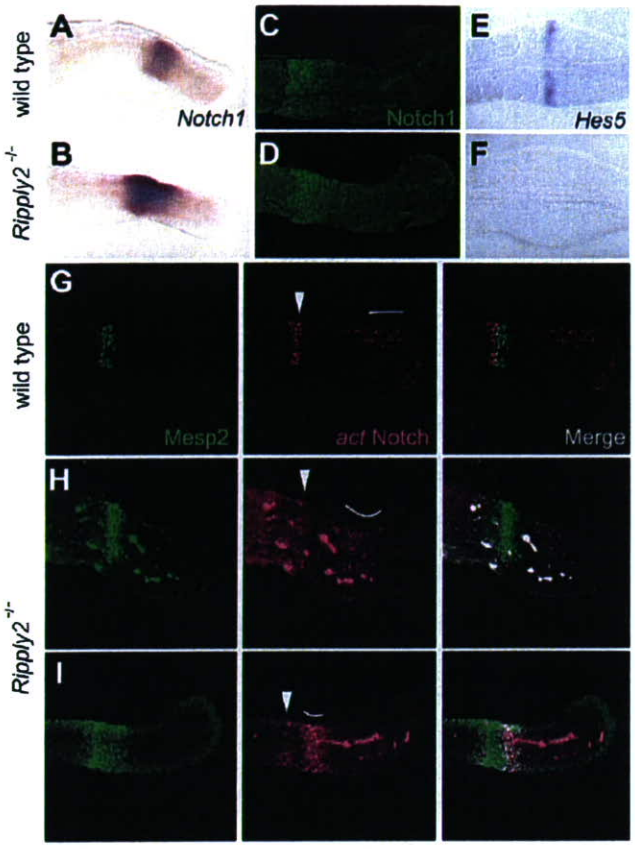

Fig. 6. Notch signaling is reduced in the anterior PSM in the *Ripply2*$^{-/-}$ embryo. (**A-F**) *Notch1* mRNA (A, *n*=2; B, *n*=2), Notch1 protein (C, *n*=2; D, *n*=2) and *Hes5* mRNA (E, *n*=2; F, *n*=4) expression patterns were compared between wild-type (A,C,E) and *Ripply2*$^{-/-}$ (B,D,F) embryos at E11.0. (**G-I**) Double immunostaining with anti-Mesp2 (green) and anti-active Notch1 (magenta; the white lines indicate activities in the anterior PSM) antibodies using sections of wild-type (G) and *Ripply2*$^{-/-}$ (H,I) E11.0 embryos. In the *Ripply2*$^{-/-}$ background, Mesp2 expression is upregulated but Notch activity is reduced.

The *Ripply2*-knockout mouse exhibits a rostralized phenotype

Because Mesp2 confers rostral properties to the somites and is involved in the formation of the somite boundary, we speculated whether Ripply2 might function in this Mesp2 pathway during somitogenesis. To elucidate this possibility, we generated *Ripply2*-knockout mice using ES cell-mediated gene targeting (Fig. 3A). Since the heterozygous mice were found to be normal, we performed timed intercross matings to analyze the phenotypes of the homozygotes. As expected from the expression patterns, the *Ripply2*$^{-/-}$ embryos failed to proceed through normal somitogenesis and the embryos displayed no clear segmental borders (Fig. 4A-D). These homozygous mice also died soon after birth. The morphology of the 17.5-dpc fetus was found to be similar to that of the *Mesp2*-null embryo, with a short trunk and tail (Fig. 3B) (Saga et al., 1997). However, the vertebral phenotype of the *Ripply2*$^{-/-}$ embryos, as revealed by skeletal staining, differed from that of *Mesp2*-null embryos as it features extensive fusion of the pedicles in the neural arches owing to the caudalized characteristics of the somitic mesoderm (Saga et al., 1997).

The *Ripply2*$^{-/-}$ mouse fetus showed fewer pedicles of neural arches (Fig. 4E,F), and the phenotype resembled that of the presenilin 1 (*Psen1*)-null mouse (Fig. 4G), which lacks Notch signaling (Koizumi et al., 2001). The findings of our gene expression studies using both rostral and caudal molecular markers are consistent with these skeletal defects. In *Ripply2*$^{+/-}$ embryos, the expression of the caudal markers *Uncx4.1* and *Dll1* in the segmented somites was restricted to the caudal compartments of the somites (Fig. 5A,C). The expression of these genes is increased and more expansive in *Mesp2*-null embryos (Takahashi et al., 2000), but was greatly reduced in the *Ripply2*-null embryos, (Fig. 5B,D). In addition, no *Dll1* stripe could be observed within the somitic region or in the anterior PSM, although the expression in the posterior PSM was intact in the *Ripply2*$^{-/-}$ embryo (Fig. 5D). By contrast, the rostral markers were found to be present in the *Ripply2*$^{-/-}$ embryo (Fig. 5E-H). *Tbx18*, which is known to be involved in the maintenance of the rostral properties of the somites (Bussen et al., 2004; Kraus et al., 2001), was expressed in the rostral compartment of the segmented somites (Fig. 5E). In *Ripply2*$^{-/-}$ embryos, this expression was expanded throughout the entire somite region and no clear segmental pattern was evident (Fig. 5F). In addition, *Epha4* was expressed in the rostral compartment of S0 and S1 somites in the *Ripply2*$^{+/-}$ embryo (Fig. 5G), and this expression in the *Ripply2*$^{-/-}$ embryo was increased and the expression domain expanded as compared with the wild type (Fig. 5H). We thus conclude that the *Ripply2*-null mouse displays a rostralized phenotype.

Ripply2 is a negative regulator of *Mesp2* expression

As we have previously reported, the rostro-caudal polarity of the somites is generated by the interaction between Mesp2 and the Notch signaling pathway in the anterior PSM (Morimoto et al., 2005). To identify the underlying cause of the rostralized phenotype in the *Ripply2*-null embryo, the *Mesp2* gene expression profile was examined. During somitogenesis in the anterior PSM, both wild-type and *Ripply2*$^{+/-}$ embryos generally showed either a single *Mesp2* expression band of variable width or no band, depending on the cyclic expression stage (Fig. 5I and data not shown). However, we observed that *Mesp2* is expressed in the *Ripply2*$^{-/-}$ embryo as either one or two bands (Fig. 5J). In other words, an additional band was frequently observed in the more-rostral region (four out of six examined). In addition, we did not observe any *Ripply2*$^{-/-}$ embryos without *Mesp2* expression, suggesting either that *Mesp2* expression is prolonged or that the *Mesp2* transcripts are stabilized in a *Ripply2*$^{-/-}$ background. To distinguish these possibilities, we performed in situ hybridization using an intron probe. Although the signal obtained was low, we frequently detected two bands in the *Ripply2*$^{-/-}$ embryos (Fig. 5L; in all three examined), but only one band in the *Ripply2*$^{+/-}$ embryos (Fig. 5K). Hence, the transcription of *Mesp2* appears to be prolonged in the absence of Ripply2, although the possibility that differences exist in their mRNA stability cannot yet be excluded.

We next examined how the expression of the Mesp2 protein is influenced in the *Ripply2*$^{-/-}$ background. As we have shown previously, Mesp2-venus can be used to visualize functional Mesp2 proteins in vivo because the homozygous knock-in mouse is viable and shows normal somitogenesis (Morimoto et al., 2005). In a typical case, a single Mesp2-venus band was detectable in the area just caudal to the next presumptive segmental border in the *Ripply2*$^{+/-}$ background (Fig. 5M). However, in the *Ripply2*$^{-/-}$ embryo, two broader and interconnected bands could be discerned (Fig. 5N). These data

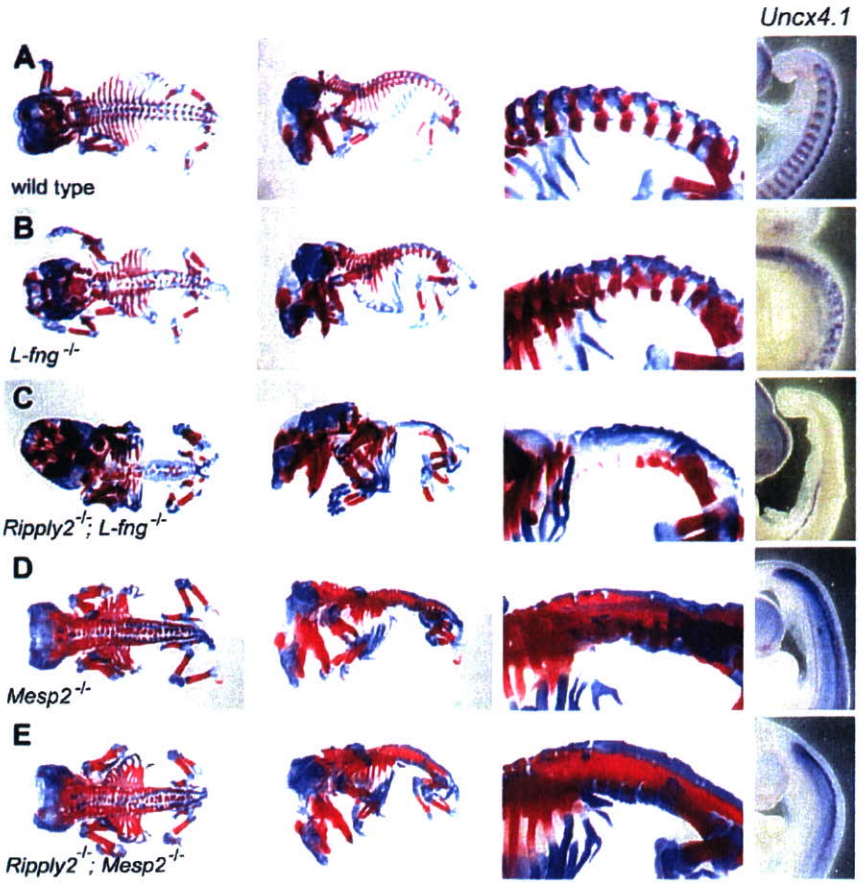

Fig. 7. Genetic analyses using double-knockouts of *Ripply2* and either *Lfng* or *Mesp2*. The skeletal morphologies and *Uncx4.1* expression patterns were compared among wild-type (**A**), *Lfng*-null (**B**), *Ripply2/Lfng* double-null (**C**), *Mesp2*-null (**D**) and *Ripply2/Mesp2* double-null (**E**) E17.5 fetuses or E9.5 embryos. The skeletal defects in the *Ripply2*$^{-/-}$ fetus were found to be further enhanced by the additional loss of *Lfng*, and the pedicles of the neural arches were almost completely absent in this compound-null fetus (C). By contrast, the *Ripply2/Mesp2* double-null fetus (E) shows a similar morphology to that of the *Mesp2* single-null fetus (D). The *Uncx4.1* expression pattern was independently examined at E10.5 (A, *n*=2; B, *n*=2; C, *n*=1) and E9.5 (A, *n*=4; B, *n*=2; C, *n*=2; D, *n*=4; E, *n*=2). Only representative images of E9.5 embryos are shown.

suggest that *Mesp2* is negatively regulated by Ripply2, and that these factors form a negative-feedback loop to restrict the levels of Mesp2.

We previously reported that *Lfng* expression is activated by Mesp2 in the anterior PSM and is subsequently involved in the suppression of Notch signaling. Moreover, *Lfng* expression shows a cyclic wave-like pattern in the posterior PSM, but its expression in the anterior PSM is similar to that of *Mesp2* in *Ripply2*$^{+/-}$ embryos. The width of this *Lfng* band becomes thinner before disappearing from the rostral end of the expression domain in the *Ripply2*$^{+/-}$ embryo (Fig. 5O). However, in the *Ripply2*$^{-/-}$ embryos, the anterior-most *Lfng* band was found to be wider and to persist for much longer as compared with the *Ripply2*$^{+/-}$ embryos (Fig. 5P). This persistent expression of *Lfng* was also evident from 20-minute explant culture experiments with a half-PSM (Fig. 5Q,R). These results suggest that Notch signaling might be suppressed, even in the presumptive caudal compartment of the somites, by prolonged Mesp2 and/or Lfng expression in the *Ripply2*$^{-/-}$ embryo.

Mesp2, but not Lfng, is responsible for the Notch suppression necessary for rostro-caudal patterning

In somite-stage embryos, Notch activity oscillates in the posterior PSM and stabilizes as a clear stripe in the anterior PSM with elevated activity (Huppert et al., 2005; Morimoto et al., 2005). To further understand the molecular events operating in the anterior PSM of *Ripply2*$^{-/-}$ embryos, we first examined the expression of *Notch1* mRNA (Fig. 6A,B) and Notch1 protein (Fig. 6C,D) in these embryos. Interestingly, these expression patterns were found to be expanded in the anterior PSM in the *Ripply2*$^{-/-}$ embryo (Fig. 6B,D), but the Notch activity appeared to be lost as judged from the fact that the expression of *Hes5*, a Notch target gene (Ohtsuka et al., 1999), was absent (Fig. 6E,F). To further confirm this reduced Notch1 activity and its relationship to Mesp2 expression, we conducted double immunostaining analysis using anti-active Notch1 and anti-Mesp2 antibodies in both wild-type and *Ripply2*$^{-/-}$ embryos. In the wild-type embryos, the Notch activity in the anterior PSM exhibited a sharp boundary with Mesp2 that determines the next segmental boundary (Fig. 6G). In addition, the contrast between Notch activities leads to the generation of future rostral and caudal compartments of the somites, whereby the Notch active site becomes the future caudal compartment. In the *Ripply2*$^{-/-}$ embryo, the Notch1 signals oscillated normally in the posterior PSM (Fig. 6H,I). However, the elevation of Notch activity in the anterior PSM appeared to be repressed in these null embryos, whereas the Mesp2 expression banding was found to upregulated, as shown previously (Fig. 6H,I).

Since the expression of *Lfng* is under the control of Mesp2, we speculated that the suppression of Notch signaling might be the result of the prolonged activation of *Lfng* in the *Ripply2*$^{-/-}$ embryo. To test this possibility, we generated a *Ripply2/Lfng* double-knockout embryo from which we prepared skeletal specimens, and then examined the somite properties by analyzing the expression of the caudal molecular marker *Uncx4.1* (Fig. 7). Intriguingly, the vertebral morphology of the *Ripply2/Lfng*

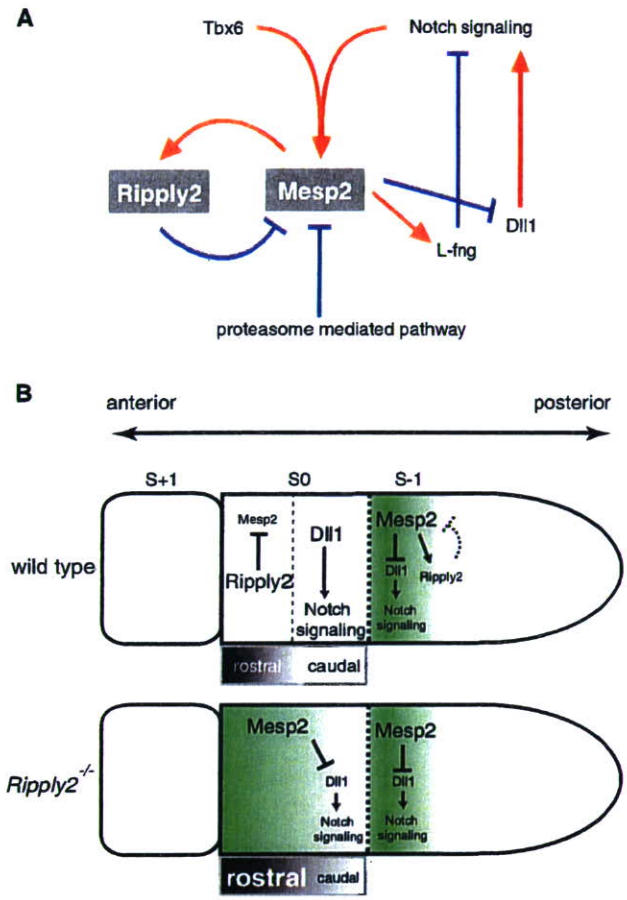

Fig. 8. Genetic cascades in the anterior PSM regulating somitogenesis. (**A**) Schematic of the positive (red line) and negative (blue line) regulation surrounding Mesp2. The transcription of *Mesp2* is enhanced by both Notch signaling and Tbx6. At the same time, Mesp2 suppresses Notch signaling by activating *Lfng* and suppressing *Dll1* expression. Mesp2 proteins are also rapidly degraded via a proteasome-dependent pathway. We herein propose a new negative regulatory system for Mesp2 via Ripply2. (**B**) Schematic illustrating how the rostro-caudal polarity is established or disrupted in the anterior PSM of the wild type and *Ripply2*$^{-/-}$ mutants. In the anterior PSM, Mesp2 is localized in the rostral compartment of S–1 and suppresses Notch signaling through the suppression of *Dll1*. By contrast, in the caudal compartment of S0, both *Dll1* expression and Notch signaling are retained because of the lack of Mesp2. In the *Ripply2*$^{-/-}$ embryo, Mesp2 expression persists for a longer period in both the rostral and caudal compartments, although the suppression on Notch signaling is incomplete. This results in the expansion of the rostral properties within the somites.

double-knockout mouse was not recovered, and was more rostralized as compared with either the *Ripply2*$^{-/-}$ (compare Fig. 4F with Fig. 7C) or *Lfng*-null fetus (Fig. 7B). The expression of *Uncx4.1* was also not recovered by the additional loss of Lfng (compare Fig. 5B with Fig. 7C), and was found to be completely diminished in the double-knockout embryos.

To determine whether the suppression of Notch signaling is mainly due to the function of Mesp2, we also generated *Mesp2/Ripply2* double-null mice and analyzed the resulting skeletal phenotypes. As expected, the vertebral morphology of these fetuses was found to be very similar to the *Mesp2* single-null fetus, and exhibited a caudalized phenotype (Fig. 7D,E). The expression of *Uncx4.1* was also upregulated to similar levels as in the *Mesp2*-null embryo (Fig. 7E). These results clearly showed that Mesp2 suppresses the expression of this gene independent of Ripply2, and that the defect observed in the *Ripply2*$^{-/-}$ mouse can be attributed to the function of Mesp2.

DISCUSSION

Our current study establishes the hypothesis that the negative-feedback regulation of Mesp2 by Ripply2 constitutes a core component of the regulatory network involved in establishing rostro-caudal patterning. The periodicity of somitogenesis is established by mechanisms based on the negative regulation of several genes in the mouse posterior PSM (Rida et al., 2004), in which the clock genes *Hes7* and *Lfng* are negatively regulated by several mechanisms, including transcriptional suppression, protein degradation and destabilization of mRNA (Bessho et al., 2003; Chen et al., 2005; Cole et al., 2002; Hirata et al., 2004; Morales et al., 2002). In the anterior PSM, the levels of Mesp2 are strictly regulated to achieve the periodic suppression of Notch signaling, and also to establish the correct rostro-caudal polarity. During this activation step, the cooperation between Tbx6 and cyclic activated Notch-signaling is crucial for the periodic induction of *Mesp2* (Yasuhiko et al., 2006) (Fig. 8A). However, these processes must be regulated by both activation and inhibition. Previously, we reported that Mesp2 is regulated negatively by the proteasome pathway (Morimoto et al., 2006). In addition, our current study has identified Ripply2 as a potent negative regulator of *Mesp2* transcription, and as a factor that is required for the correct establishment of rostro-caudal patterning. In the absence of Ripply2, Mesp2 expression is maintained over a longer period and leads to the suppression of caudal properties (Fig. 8B). It is noteworthy in this regard that Ripply2 might function exclusively to negatively regulate Mesp2, because the phenotype of the *Ripply2*-knockout mouse is almost completely reversed by the additional loss of Mesp2.

The *Ripply2*-null mutant exhibits not only an expansion of rostral marker genes but also a reduction in the expression of caudal markers. Immunohistochemical analysis further revealed a decrease in the activated form of Notch1 in the anterior PSM in these *Ripply2*-null embryos. Previously, we have shown that Mesp2 suppresses Notch signaling to establish segmental boundaries via the activation of Lfng. However, Lfng appears not to be crucial for the suppression of Notch signaling in the *Ripply2*-null embryo as this suppression was not rescued by the additional loss of Lfng, and, in fact, this results in a further reduction in Notch signaling activity. We speculate that this is caused by the function of Lfng during Mesp2 distribution, based upon our observations of the Mesp2-venus knock-in mouse. In the wild-type embryo, the Mesp2-venus expression pattern shows a clear gradient, being higher in the presumptive rostral compartment. However, in the absence of Lfng, such a biased gradient is not generated, and the Mesp2-venus pattern shows a diffuse distribution in this background (our unpublished data). The phenotype of the *Ripply2/Lfng* double-knockout mouse appears also to reflect this distribution defect. In this double-null mouse, the expression of Mesp2 is prolonged owing to the lack of Ripply2, and is distributed across a much wider area along the anterior-posterior axis because of the lack of Lfng. This in turn enhances the function of Mesp2 that suppresses Notch signaling in the anterior PSM, and results in the somites becoming completely rostralized in these double mutants.

The mechanisms underlying the suppression of Mesp2 by Ripply2 are currently unknown. Ripply2 appears to be required for the termination of Mesp2 expression at an appropriate time. Moreover, because Ripply2 has no apparent DNA-binding domain, it is plausible to assume that it suppresses *Mesp2* by recruiting the Groucho homolog Tle1 and/or Tle3 via the WRPW motif, as revealed previously by in vitro assays in both zebrafish and mouse (Kawamura et al., 2005) (data not shown). *Tle1* and *Tle3* are known to be expressed in the PSM, but their expression patterns are not segmental (Dehni et al., 1995) (our unpublished data), and no loss-of-function studies have yet been reported. In the zebrafish, *ripply1* morphants also display upregulation of *mespb* in their somitic regions, and this is accompanied by the upregulation of *tbx24*, *deltaC* and *deltaD*. This might also account for the upregulation of *mespb* (Kawamura et al., 2005). We have previously identified a 300 bp upstream region of the *Mesp2* gene as a promoter-enhancer sequence required for the faithful expression of *Mesp2* in the anterior PSM where T-box factor binding in combination with Notch signaling is involved in the gene activation (Yasuhiko et al., 2006). However, Tbx6 expression is unchanged (data not shown) and the *Dll1* expression profile is somewhat decreased in the *Ripply2*-null embryos. Hence, although the impact of the loss of Ripply proteins upon Mesp gene expression appears to be similar between mouse and zebrafish, the underlying mechanisms might well be different.

We are particularly thankful to Yuki Takahashi and Aya Satoh for their valuable technical support and for maintaining the mice used in this study. We thank Randy Johnson for generously providing the *Lfng*-knockout mouse and Masaru Tamura for permitting us to use the FreeStyle 293 expression system. This work was supported by Grants-in-Aid for Science Research on Priority Areas (B), the Organized Research Combination System and National BioResource Project of the Ministry of Education, Culture, Sports, Science and Technology, Japan.

Supplementary material

Supplementary material for this article is available at
http://dev.biologists.org/cgi/content/full/134/8/1561/DC1

References

Bessho, Y., Sakata, R., Komatsu, S., Shiota, K., Yamada, S. and Kageyama, R. (2001). Dynamic expression and essential functions of Hes7 in somite segmentation. *Genes Dev.* **15**, 2642-2647.

Bessho, Y., Hirata, H., Masamizu, Y. and Kageyama, R. (2003). Periodic repression by the bHLH factor Hes7 is an essential mechanism for the somite segmentation clock. *Genes Dev.* **17**, 1451-1456.

Bettenhausen, B., Hrabe de Angelis, M., Simon, D., Guenet, J. L. and Gossler, A. (1995). Transient and restricted expression during mouse embryogenesis of Dll1, a murine gene closely related to Drosophila Delta. *Development* **121**, 2407-2418.

Borycki, A. G. and Emerson, C. P., Jr (2000). Multiple tissue interactions and signal transduction pathways control somite myogenesis. *Curr. Top. Dev. Biol.* **48**, 165-224.

Brand-Saberi, B. and Christ, B. (2000). Evolution and development of distinct cell lineages derived from somites. *Curr. Top. Dev. Biol.* **48**, 1-42.

Bussen, M., Petry, M., Schuster-Gossler, K., Leitges, M., Gossler, A. and Kispert, A. (2004). The T-box transcription factor Tbx18 maintains the separation of anterior and posterior somite compartments. *Genes Dev.* **18**, 1209-1221.

Chen, J., Kang, L. and Zhang, N. (2005). Negative feedback loop formed by Lunatic fringe and Hes7 controls their oscillatory expression during somitogenesis. *Genesis* **43**, 196-204.

Cole, S. E., Levorse, J. M., Tilghman, S. M. and Vogt, T. F. (2002). Clock regulatory elements control cyclic expression of Lunatic fringe during somitogenesis. *Dev. Cell* **3**, 75-84.

Dehni, G., Liu, Y., Husain, J. and Stifani, S. (1995). TLE expression correlates with mouse embryonic segmentation, neurogenesis, and epithelial determination. *Mech. Dev.* **53**, 369-381.

Dubrulle, J. and Pourquie, O. (2004). Coupling segmentation to axis formation. *Development* **131**, 5783-5793.

Haraguchi, S., Kitajima, S., Takagi, A., Takeda, H., Inoue, T. and Saga, Y. (2001). Transcriptional regulation of Mesp1 and Mesp2 genes: differential usage of enhancers during development. *Mech. Dev.* **108**, 59-69.

Hirata, H., Bessho, Y., Kokubu, H., Masamizu, Y., Yamada, S., Lewis, J. and Kageyama, R. (2004). Instability of Hes7 protein is crucial for the somite segmentation clock. *Nat. Genet.* **36**, 750-754.

Huppert, S. S., Ilagan, M. X., De Strooper, B. and Kopan, R. (2005). Analysis of Notch function in presomitic mesoderm suggests a gamma-secretase-independent role for presenilins in somite differentiation. *Dev. Cell* **8**, 677-688.

Iulianella, A., Melton, K. R. and Trainor, P. A. (2003). Somitogenesis: breaking new boundaries. *Neuron* **40**, 11-14.

Kanno, J., Aisaki, K., Igarashi, K., Nakatsu, N., Ono, A., Kodama, Y. and Nagao, T. (2006). "Per cell" normalization method for mRNA measurement by quantitative PCR and microarrays. *BMC Genomics* **7**, 64.

Kawamura, A., Koshida, S., Hijikata, H., Ohbayashi, A., Kondoh, H. and Takada, S. (2005). Groucho-associated transcriptional repressor ripply1 is required for proper transition from the presomitic mesoderm to somites. *Dev. Cell* **9**, 735-744.

Koizumi, K., Nakajima, M., Yuasa, S., Saga, Y., Sakai, T., Kuriyama, T., Shirasawa, T. and Koseki, H. (2001). The role of presenilin 1 during somite segmentation. *Development* **128**, 1391-1402.

Kraus, F., Haenig, B. and Kispert, A. (2001). Cloning and expression analysis of the mouse T-box gene Tbx18. *Mech. Dev.* **100**, 83-86.

Leitges, M., Neidhardt, L., Haenig, B., Herrmann, B. G. and Kispert, A. (2000). The paired homeobox gene Uncx4.1 specifies pedicles, transverse processes and proximal ribs of the vertebral column. *Development* **127**, 2259-2267.

Monsoro-Burq, A. H. and Le Douarin, N. (2000). Duality of molecular signaling involved in vertebral chondrogenesis. *Curr. Top. Dev. Biol.* **48**, 43-75.

Morales, A. V., Yasuda, Y. and Ish-Horowicz, D. (2002). Periodic Lunatic fringe expression is controlled during segmentation by a cyclic transcriptional enhancer responsive to notch signaling. *Dev. Cell* **3**, 63-74.

Morimoto, M., Takahashi, Y., Endo, M. and Saga, Y. (2005). The Mesp2 transcription factor establishes segmental borders by suppressing Notch activity. *Nature* **435**, 354-359.

Morimoto, M., Kiso, M., Sasaki, N. and Saga, Y. (2006). Cooperative Mesp activity is required for normal somitogenesis along the anterior-posterior axis. *Dev. Biol.* **300**, 687-698.

Nakajima, Y., Morimoto, M., Takahashi, Y., Koseki, H. and Saga, Y. (2006). Identification of Epha4 enhancer required for segmental expression and the regulation by Mesp2. *Development* **133**, 2517-2525.

Nomura-Kitabayashi, A., Takahashi, Y., Kitajima, S., Inoue, T., Takeda, H. and Saga, Y. (2002). Hypomorphic Mesp allele distinguishes establishment of rostrocaudal polarity and segment border formation in somitogenesis. *Development* **129**, 2473-2481.

Ohtsuka, T., Ishibashi, M., Gradwohl, G., Nakanishi, S., Guillemot, F. and Kageyama, R. (1999). Hes1 and Hes5 as notch effectors in mammalian neuronal differentiation. *EMBO J.* **18**, 2196-2207.

Pourquie, O. (2003). The segmentation clock: converting embryonic time into spatial pattern. *Science* **301**, 328-330.

Rida, P. C., Le Minh, N. and Jiang, Y. J. (2004). A Notch feeling of somite segmentation and beyond. *Dev. Biol.* **265**, 2-22.

Saga, Y. and Takeda, H. (2001). The making of the somite: molecular events in vertebrate segmentation. *Nat. Rev. Genet.* **2**, 835-845.

Saga, Y., Hata, N., Koseki, H. and Taketo, M. M. (1997). Mesp2: a novel mouse gene expressed in the presegmented mesoderm and essential for segmentation initiation. *Genes Dev.* **11**, 1827-1839.

Sakai, K. and Miyazaki, J. (1997). A transgenic mouse line that retains Cre recombinase activity in mature oocytes irrespective of the cre transgene transmission. *Biochem. Biophys. Res. Commun.* **237**, 318-324.

Takahashi, Y., Koizumi, K., Takagi, A., Kitajima, S., Inoue, T., Koseki, H. and Saga, Y. (2000). Mesp2 initiates somite segmentation through the Notch signalling pathway. *Nat. Genet.* **25**, 390-396.

Takahashi, Y., Inoue, T., Gossler, A. and Saga, Y. (2003). Feedback loops comprising Dll1, Dll3 and Mesp2, and differential involvement of Psen1 are essential for rostrocaudal patterning of somites. *Development* **130**, 4259-4268.

Yagi, T., Tokunaga, T., Furuta, Y., Nada, S., Yoshida, M., Tsukada, T., Saga, Y., Takeda, N., Ikawa, Y. and Aizawa, S. (1993). A novel ES cell line, TT2, with high germline-differentiating potency. *Anal. Biochem.* **214**, 70-76.

Yasuhiko, Y., Haraguchi, S., Kitajima, S., Takahashi, Y., Kanno, J. and Saga, Y. (2006). Tbx6-mediated Notch signaling controls somite-specific Mesp2 expression. *Proc. Natl. Acad. Sci. USA* **103**, 3651-3656.

Arch Pharm Res Vol 30, No 4, 444-452, 2007

Archives of Pharmacal Research
http://apr.psk.or.kr

Gene Expression Profiles in T24 Human Bladder Carcinoma Cells by Inhibiting an L-type Amino Acid Transporter, LAT1

Shadi Baniasadi[1,2], Arthit Chairoungdua[2], Yuji Iribe[2], Yoshikatsu Kanai[2], Hitoshi Endou[2], Ken-ichi Aisaki[3], Katsuhide Igarashi[3], and Jun Kanno[3]

[1]National Research Institute of Tuberculosis and Lung Diseases, Shaheed Beheshti University of Medical Science, Tehran, Iran, [2]Department of Pharmacology and Toxicology, Kyorin University School of Medicine, 6-20-2 Shinkawa, Mitaka, Tokyo 181-8611, Japan, and [3]Division of Cellular & Molecular Toxicology, National Institute of Health Sciences, Kamiyoga 1-18-1, Setagaya-ku, Tokyo 158-8501, Japan

(Received November 13, 2006)

Inhibition of LAT1 (L-type amino acid transporter 1) activity in tumor cells could be effective in the inhibition of tumor cell growth by depriving tumor cells of essential amino acids. Because of the high level of expression of LAT1 in tumor cells, LAT1 inhibitors would be useful for anticancer therapy in suppressing tumor growth without affecting normal tissues. In recent years, cDNA microarray technique is useful technology for anticancer drug development. It allows identifying and characterizing new targets for developments in cancer drug therapy through the understanding genes involved in drug action. The present study was designed to investigate gene expression profile induced by LAT1 inhibitor using gene chip technology. Human bladder carcinoma cells (T24 cells) were treated with classical system L inhibitor 2-aminobicyclo-(2, 2, 1)-heptane-2-carboxylic acid (BCH). Gene chip experiment was applied for treated and untreated cells after 3 and 12 h. Two independent experiments with a high degree of concordance identified the altered expression of 151 and 200 genes after 3 and 12 h BCH treatment. Among these genes, 132 and 13 were up-regulated and 19 and 187 were down-regulated by 3 and 12 h BCH treatment respectively. We found that BCH affected the expression of a large number of genes that are related to the control of cell survival and physiologic behaviors. These data are useful for understanding of intracellular signaling of cell growth inhibition induced by LAT1 inhibitors as candidate for anticancer drug therapy.

Key words: BCH, Gene expression, Microarray, Bladder carcinoma cells, LAT1

INTRODUCTION

System L is a major nutrient transport system responsible for the Na^+-independent transport of large neutral amino acids including several essential amino acids (Christensen, 1990; Oxender and Christensen, 1963). In malignant tumors, a system L transporter L-type amino acid transporter 1 (LAT1) is up-regulated to support tumor cell growth (Kanai *et al.*, 1998; Sang *et al.*, 1995; Wolf *et al.*, 1996; Yanagida *et al.*, 2001) . It is proposed that the manipulation of system L activity, in particular that of LAT1, would have therapeutic implications. The inhibition of LAT1 activity in tumor cells could be effective in the inhibition of tumor cell growth by depriving tumor cells of essential amino acids (Kanai and Endou, 2001). Our previous studies have revealed that T24 cells express LAT1 in the plasma membrane together with its associating protein 4F2hc that inhibited by a system L-specific inhibitor 2-aminobicyclo-(2, 2, 1)-heptane-2-carboxylic acid (BCH) (Kim *et al.*, 2002; Yanagida *et al.*, 2001). An increased understanding of molecular mechanisms of LAT1 inhibitors will lead to the development LAT1 inhibitors for anticancer drug therapy.

cDNA microarray analysis permits the simultaneous and rapid analysis of the expression of tens of thousands of genes, and, in turn, provides an opportunity for determining the effects of anticancer agents. This technology will contribute to the more accurate development of therapeutic strategies and will help to determine the molecular mechanism(s) of action of chemopreventive and/or therapeutic agents (Li and Sarkar 2002; Macgregor and Squire,

Correspondence to: Shadi Baniasadi, National Research Institute of Tuberculosis and Lung Diseases Shaheed Beheshti University of Medical Science Tehran Iran
E-mail: sbaniasadi@yahoo.com, baniasadi@nrtld.ac.ir

2002). To better understand the precise molecular mechanisms by which BCH exerts its effects on T24 bladder carcinoma cells, we utilized a cDNA microarray to interrogate the mRNA levels of 39,000 genes and to determine the gene expression profiles of T24 bladder carcinoma cells treated with BCH.

MATERIALS AND METHODS

Cell culture and growth inhibition

T24 human bladder cancer cells were cultured in the growth medium (minimum essential medium supplemented with 10% fetal bovine serum) in a 5% CO_2 atmosphere at 37°C. For growth inhibition, 60 h after seeding (during logarithmic phase) T24 cells were treated with 20 mM BCH for 3 and 12 h.

cDNA microarray analysis for gene expression profiles

T24 cells were treated with 20 mM BCH for 3 and 12 h. The rationale for choosing these time points was to capture gene expression profiles of early response genes, genes that may be involved during the onset of growth inhibition. Total RNA from each sample was isolated by Trizol (Invitrogen) and purified by RNeasy Mini Kit and RNase-free DNase Set (QIAGEN, Valencia, CA) according to the manufactures' protocols. cDNA for each sample was synthesized by using Superscript cDNA Synthesis Kit (Invitrogen) using T7-(dT)24 primer instead of the oligo (dT) provided in the kit. The biotin-labeled cRNA was transcripted in vitro from cDNA using a BioArray HighYield RNA Transcript Labeling Kit (ENZO Biochem, New York, NY) and purified using an RNeasy Mini Kit. The purified cRNA was fragmented by incubation in fragmentation buffer (200 mmol/L Tris-acetate pH 8.1, 500 mmol/L KOAc, 150 mmol/L MgOAc) at 95°C for 35 min and chilled on ice. The fragmented labeled cRNA was applied to Human Genome U133 Array (Affymetrix, Santa Clara, CA), which contains 39,000 human gene cDNA probes, and hybridized to the probes in the array. After washing and staining, the arrays were scanned using a HP GeneArray Scanner (Hewlett-Packard, Palo Alto, CA). Two independent experiments were performed to verify the reproducibility of results.

Microarray data normalization and analysis

Data analysis was performed with the GeneChip Expression Analysis software (Affymetrix) and GeneSpring TM software (Silicon Genetics, Redwood, CA, U.S.A.). The differences in hybridization efficiency among arrays were equalized by intensities of spiked-in control mRNAs added to the sample in proportion to its DNA content (Kanno *et al.*, 2006). In a set of GeneChip experiments comparing the same sample hybridized to two different arrays, method-associated experimental artifacts produced less than two-fold differences between two identical samples. Thus, genes displayed over two-fold expression change were subjected to further testing. GeneChip array HG-U133A represents 22283 transcripts and the genes whose absolute call judged "present" in at least 1 sample were used for further analysis.

RESULTS

Cell growth inhibition by BCH treatment

Cell count showed that the treatment of T24 bladder cancer cells with BCH, time dependently inhibited cell proliferation (Fig. 1), demonstrating the growth inhibitory effect of BCH. These results are consistent with our previous study. This inhibition of cell proliferation could be due to altered regulation of gene expression by BCH.

Regulation of gene expression by BCH treatment

The gene expression profiles of T24 cells treated with BCH were assessed using cDNA microarray. Two inde-

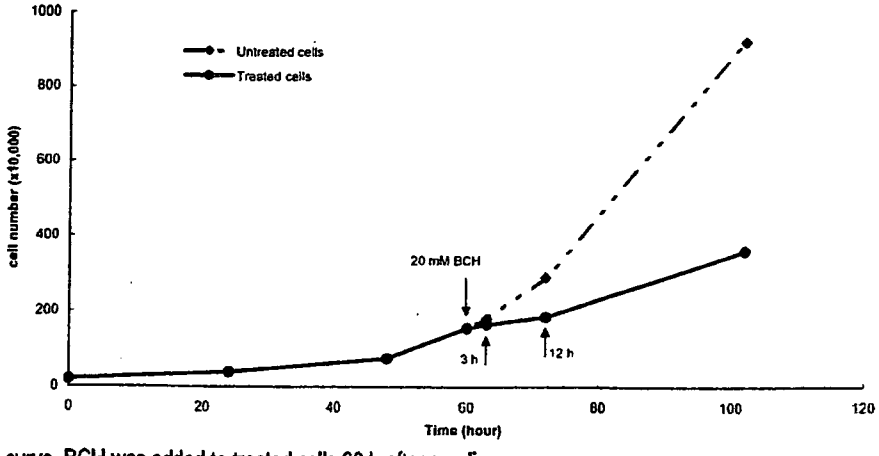

Fig. 1. T24 cell growth curve. BCH was added to treated cells 60 h after seeding.

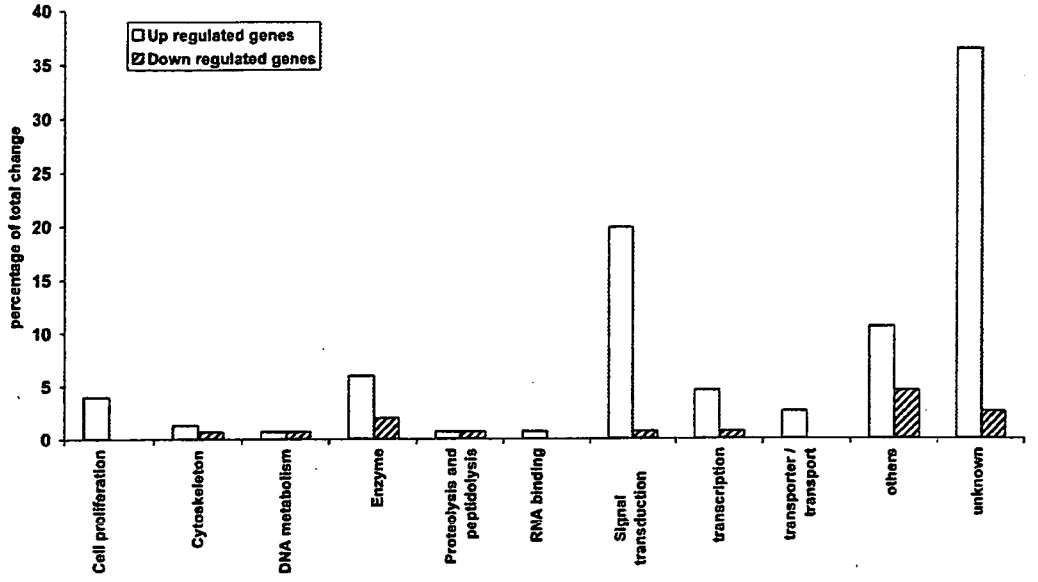

Fig. 2. Effect of BCH on gene expression after 3 h. Expression of many genes altered in T24 cells treated with BCH for 3 h.

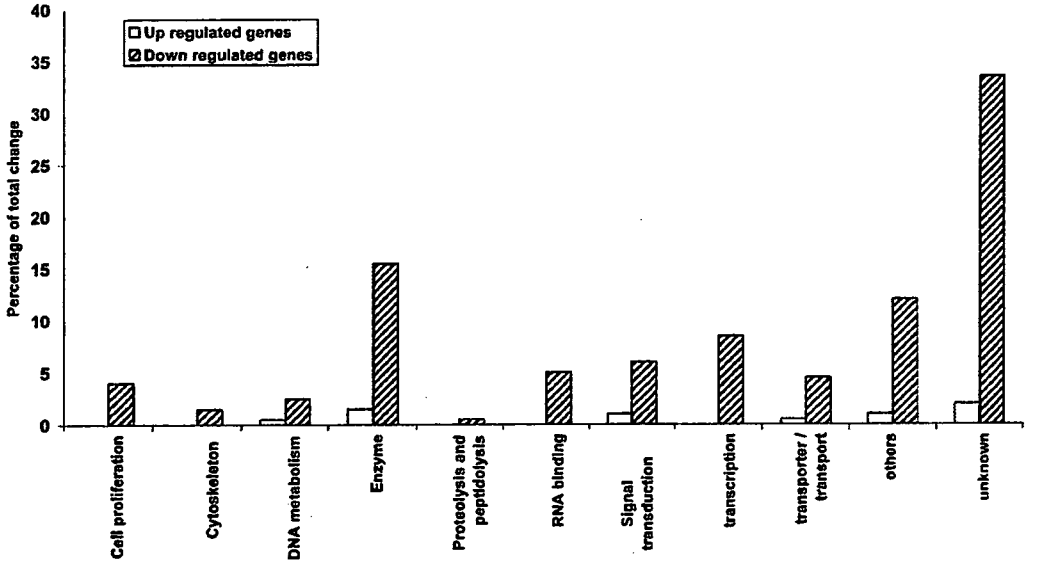

Fig 3. Effect of BCH on gene expression after 12 h. Expression of many genes altered in T24 cells treated with BCH for 12 h.

pendent experiments showed the altered expression of 151 and 200 genes at the mRNA level after 3 and 12 h BCH treatment. Among these genes, 132 and 13 were up-regulated and 19 and 187 were down-regulated by 3 and 12 h BCH treatment respectively. Expression of genes altered as early as 3 and 12 h of BCH treatment and was significantly up-regulated after 3 h and down-regulated after 12 h (Figs. 2 and 3). We found that after 3 h, BCH up-regulated genes that are involved mainly in signal transduction, enzyme reaction, transcription, cell proliferation and transport (Table I). On the other hand after 12 h, BCH down-regulated genes that are related mainly to enzyme reaction, transcription, signal transduction, RNA binding, transport, cell proliferation and DNA metabolism (Table II).

DISCUSSION

For continuous growth and proliferation, rapidly dividing tumor cells require more supply of sugars and amino acids. They are supported by the up regulation of transporters specialized for those nutrients. Transporters for essential amino acids are particularly important since they

Table I. Fold changes of specific genes in T24 cells treated with BCH for 3 h

genes	foldchange	t-test p-value
signal transduction		
Hypothetical protein	3.100	0.156
th79e05.x1 Soares_NhHMPu_S1 Homo sapiens cDNA clone IMAGE:2124896 3', mRNA sequence.	2.871	0.045
Sorting nexin 11	2.691	0.012
GABA(A) receptor-associated protein like 1	2.674	0.083
Down syndrome critical region gene 1	2.666	0.058
Interleukin 8	2.629	0.123
wd41c03.x1 Soares_NFL_T_GBC_S1 Homo sapiens cDNA clone IMAGE:2330692 3' similar to TR:O00538 O00538 F25B3.3 KINASE LIKE PROTEIN. ;, mRNA sequence.	2.596	0.439
Interleukin 8	2.534	0.087
IL2-inducible T-cell kinase	2.526	0.371
Protein kinase C, beta 1	2.427	0.151
Insulin-like growth factor binding protein 3	2.377	0.130
Vav 3 oncogene	2.267	0.053
Fibroblast growth factor 12B	2.237	0.127
CD53 antigen	2.216	0.106
MAD (mothers against decapentaplegic, Drosophila) homolog 7	2.194	0.073
GRO2 oncogene	2.186	0.020
G protein-coupled receptor 27	2.178	0.308
Adhesion glycoprotein	2.173	0.061
qq08e12.x1 Soares_NhHMPu_S1 Homo sapiens cDNA clone IMAGE:1931950 3', mRNA sequence.	2.159	0.027
Epiregulin	2.152	0.021
Gamma-aminobutyric acid (GABA) receptor, rho 2	2.143	0.159
DKFZP564L0862 protein	2.125	0.505
Insulin-like growth factor binding protein 1	2.080	0.216
GTP-binding protein overexpressed in skeletal muscle	2.074	0.056
Syntrophin, gamma 1	2.053	0.388
Adenosine A1 receptor	2.046	0.024
Inhibin, alpha	2.020	0.003
Frizzled (Drosophila) homolog 7	2.008	0.055
601763146F1 NIH_MGC_20 Homo sapiens cDNA clone IMAGE:4026010 5', mRNA sequence.	2.008	0.101
enzyme		
Cytosolic beta-glucosidase	2.668	0.209
UDP glycosyltransferase 1 family, polypeptide A1	2.355	0.014
wg36d09.x1 Soares_NSF_F8_9W_OT_PA_P_S1 Homo sapiens cDNA clone IMAGE:2367185 3', mRNA sequence.	2.287	0.072
Arginase, liver	2.201	0.339
Peptidylprolyl isomerase A (cyclophilin A)	2.166	0.423
ov13a06.x1 NCI_CGAP_Kid3 Homo sapiens cDNA clone IMAGE:1637170 3' similar to WP:R07B7.5 CE06267 ;, mRNA sequence.	2.116	0.270
cytochrome P450IIE1; Human cytochrome P450IIE1 (ethanol-inducible) gene, complete cds.	2.075	0.279
Keratin, hair, basic, 6 (monilethrix)	2.072	0.043
Protein kinase, Y-linked	2.028	0.430
transcription		
Homeo box A6	2.294	0.062
yf31g02.s1 Soares fetal liver spleen 1NFLS Homo sapiens cDNA clone IMAGE:128498 3', mRNA sequence.	2.024	0.259
Runt-related transcription factor 2	2.009	0.048

Table I. Continued

genes	foldchange	t-test p-value
transcription		
Cardiac-specific homeo box	2.095	0.170
wa17f11.x1 NCI_CGAP_Kid11 Homo sapiens cDNA clone IMAGE:2298381 3' similar to TR:Q15886 Q15886 X-LINKED NUCLEAR PROTEIN ;, mRNA sequence.	2.435	0.276
Cofactor required for Sp1 transcriptional activation, subunit 3 (130kD)	2.376	0.132
Wolf-Hirschhorn syndrome candidate 1-like 1	2.047	0.013
cell proliferation		
Tumor necrosis factor receptor superfamily, member 9	2.651	0.084
Interleukin 1, beta	2.233	0.001
Interleukin 1, alpha	2.150	0.019
Interleukin 12A (natural killer cell stimulatory factor 1, cytotoxic lymphocyte maturation factor 1, p35)	2.124	0.162
Epidermal growth factor receptor (avian erythroblastic leukemia viral (v-erb-b) oncogene homolog)	2.093	0.066
nad20g10.x1 NCI_CGAP_Lu24 Homo sapiens cDNA clone IMAGE:3366330 3', mRNA sequence.	2.031	0.087
transport		
Solute carrier family 4, sodium bicarbonate cotransporter-like, member 10	3.528	0.166
UI-H-BW0-ajo-f-12-0-UI.s1 NCI_CGAP_Sub6 Homo sapiens cDNA clone IMAGE:2732686 3', mRNA sequence.	2.468	0.423
Solute carrier family 35 (UDP-N-acetylglucosamine (UDP-GlcNAc) transporter), member 3	2.110	0.152
Solute carrier family 21 (organic anion transporter), member 3	2.031	0.030

Table II. Fold changes of specific genes in T24 cells treated with BCH for 12 h

gene	foldchange	t-test p-value
enzyme		
GDP-mannose pyrophosphorylase B	0.306	0.078
AU121975 MAMMA1 Homo sapiens cDNA clone MAMMA1001393 5', mRNA sequence.	0.319	0.235
Polymerase (DNA directed), mu	0.334	0.159
Adenylate kinase 2	0.353	0.015
F-box only protein 9	0.362	0.057
Stearoyl-CoA desaturase (delta-9-desaturase)	0.362	0.046
N-myristoyltransferase 1	0.370	0.095
Protein phosphatase 2 (formerly 2A), regulatory subunit B" (PR 72), alpha isoform and (PR 130), beta isoform	0.383	0.078
Homo sapiens Scd mRNA for stearoyl-CoA desaturase, complete cds.	0.384	0.009
qd05f07.x1 Soares_placenta_8to9weeks_2NbHP8to9W Homo sapiens cDNA clone IMAGE:1722853 3' similar to SW:ER19_HUMAN P53602 DIPHOSPHOMEVALONATE DECARBOXYLASE ;contains MER22.b1 MSR1 repetitive element ;, mRNA sequence.	0.404	0.013
602022620F1 NCI_CGAP_Brn67 Homo sapiens cDNA clone IMAGE:4158005 5', mRNA sequence.	0.406	0.020
N-acetylglucosaminidase, alpha- (Sanfilippo disease IIIB)	0.407	0.279
3-hydroxybutyrate dehydrogenase (heart, mitochondrial)	0.409	0.238
Creatine kinase, mitochondrial 2 (sarcomeric)	0.440	0.135
Phosphodiesterase 4D, cAMP-specific (dunce (Drosophila)-homolog phosphodiesterase E3)	0.441	0.020
qi08f09.x1 Soares_NhHMPu_S1 Homo sapiens cDNA clone IMAGE:1855913 3', mRNA sequence.	0.454	0.071
AL525798 LTI_NFL003_NBC3 Homo sapiens cDNA clone CS0DC013YB08 5 prime, mRNA sequence.	0.454	0.020
KIAA0015 gene product	0.455	0.043
Glutaryl-Coenzyme A dehydrogenase	0.467	0.082
Polynucleotide kinase 3'-phosphatase	0.470	0.079
Enolase 2, (gamma, neuronal)	0.471	0.008
xn86c10.x1 Soares_NFL_T_GBC_S1 Homo sapiens cDNA clone IMAGE:2701362 3' similar to TR:Q99766 Q99766 HYPOTHETICAL 15.7 KD PROTEIN. ; mRNA sequence.	0.481	0.112

Table II. Continued

gene	foldchange	t-test p-value
enzyme		
Serine hydroxymethyltransferase 1 (soluble)	0.483	0.092
Crystallin, zeta (quinone reductase)-like 1	0.486	0.042
xd94e03.x1 Soares_NFL_T_GBC_S1 Homo sapiens cDNA clone IMAGE:2605276 3' similar to WP:Y116A8C.27 CE23335 ;, mRNA sequence.	0.488	0.213
Aminoacylase 1	0.488	0.016
H.sapiens pseudogene for mitochondrial ATP synthase c subunit (P2 form).	0.491	0.088
zi27a06.s1 Soares_fetal_liver_spleen_1NFLS_S1 Homo sapiens cDNA clone IMAGE:431986 3', mRNA sequence.	0.491	0.061
Fatty-acid-Coenzyme A ligase, long-chain 3	0.492	0.069
Triosephosphate isomerase 1	0.494	0.322
Tumor necrosis factor receptor superfamily, member 6b, decoy	0.495	0.000
transcription		
Paired box gene 3 (Waardenburg syndrome 1)	0.342	0.260
Paired box gene 8	0.423	0.218
AU118165 HEMBA1 Homo sapiens cDNA clone HEMBA1003008 5', mRNA sequence.	0.466	0.057
Core promoter element binding protein	0.447	0.016
Death effector domain-containing	0.484	0.028
Trinucleotide repeat containing 11 (THR-associated protein, 230 kDa subunit)	0.498	0.002
NS1-binding protein	0.335	0.018
Hypothetical protein	0.484	0.031
602437464F1 NIH_MGC_46 Homo sapiens cDNA clone IMAGE:4555622 5', mRNA sequence.	0.486	0.027
601872674F1 NIH_MGC_54 Homo sapiens cDNA clone IMAGE:4096483 5', mRNA sequence.	0.432	0.002
Cofactor required for Sp1 transcriptional activation, subunit 9 (33kD)	0.472	0.157
Zinc finger protein 254	0.489	0.374
Ring finger protein 1	0.404	0.154
Nuclear respiratory factor 1	0.376	0.111
HSPC028 protein	0.486	0.009
KIAA0664 protein	0.496	0.031
signal transduction		
Regulator of G-protein signalling 4	0.109	0.029
Integrin, alpha 9	0.164	0.015
CAMP responsive element modulator	0.255	0.158
Endothelin receptor type B	0.302	0.011
AL514445 LTI_NFL006_PL2 Homo sapiens cDNA clone CL0BB010ZF08 3 prime, mRNA sequence.	0.322	0.008
Ankyrin 1, erythrocytic	0.340	0.094
wu94e06.x1 NCI_CGAP_Kid3 Homo sapiens cDNA clone IMAGE:2527714 3' similar to gb:U07358 MIXED LINEAGE KINASE 2 (HUMAN);, mRNA sequence.	0.342	0.098
ADP-ribosylation factor related protein 1	0.345	0.030
Melanoma cell adhesion molecule	0.351	0.053
7o43e03.x1 NCI_CGAP_Kid11 Homo sapiens cDNA clone IMAGE:3577036 3', mRNA sequence.	0.431	0.095
LIM domain only 7	0.439	0.045
Enigma (LIM domain protein)	0.492	0.036
RNA binding		
qb33c06.x1 Soares_pregnant_uterus_NbHPU Homo sapiens cDNA clone IMAGE:1698058 3', mRNA sequence.	0.215	0.055
RNA binding motif protein 12	0.386	0.007

Table II. Continued

gene	foldchange	t-test p-value
RNA binding		
Polyadenylate binding protein-interacting protein 1	0.411	0.029
Splicing factor, arginine/serine-rich 6	0.419	0.003
AU146237 HEMBA1 Homo sapiens cDNA clone HEMBA1007233 3', mRNA sequence.	0.422	0.013
Polyadenylate binding protein-interacting protein 1	0.458	0.058
Splicing factor, arginine/serine-rich 7 (35kD)	0.472	0.060
DEAD-box protein abstrakt	0.493	0.035
Mitochondrial ribosomal protein L12	0.495	0.138
Heterogeneous nuclear ribonucleoprotein D-like	0.497	0.025
transport		
wc46f12.x1 NCI_CGAP_Pr28 Homo sapiens cDNA clone IMAGE:2321711 3' similar to TR:O14564 O14564 HYPOTHETICAL 67.1 KD PROTEIN. ;, mRNA sequence.	0.338	0.072
Uncoupling protein 2 (mitochondrial, proton carrier)	0.385	0.020
Adaptor-related protein complex 3, sigma 2 subunit	0.278	0.110
Solute carrier family 4, anion exchanger, member 2 (erythrocyte membrane protein band 3-like 1)	0.408	0.134
Hypothetical protein FLJ14038	0.469	0.002
Solute carrier family 4, sodium bicarbonate cotransporter-like, member 10	0.395	0.124
N amino acid transporter 3	0.451	0.072
Solute carrier family 25 (mitochondrial carrier; oxoglutarate carrier), member 11	0.467	0.017
Solute carrier family 19 (folate transporter), member 1	0.490	0.068
cell proliferation		
Deoxyhypusine synthase	0.175	0.026
Deoxyhypusine synthase	0.372	0.039
ba69f11.x1 NIH_MGC_20 Homo sapiens cDNA clone IMAGE:2905677 3' similar to SW:CL6_RAT Q08755 INSULIN-INDUCED GROWTH RESPONSE PROTEIN CL-6 ;, mRNA sequence.	0.437	0.008
Cyclin H	0.455	0.043
Bridging integrator 1	0.487	0.071
V-Ki-ras2 Kirsten rat sarcoma 2 viral oncogene homolog	0.489	0.171
Deoxyhypusine synthase	0.494	0.031
U69567 Soares infant brain 1NIB Homo sapiens cDNA clone c-2mell, mRNA sequence.	0.499	0.072
DNA metabolism		
BRCA1-interacting protein 1; BRCA1-associated C-terminal helicase 1	0.410	0.028
Uracil-DNA glycosylase	0.434	0.102
Nth (E.coli endonuclease III)-like 1	0.443	0.017
DNA (cytosine-5-)-methyltransferase 2	0.469	0.209
602504673F1 NIH_MGC_77 Homo sapiens cDNA clone IMAGE:4617907 5', mRNA sequence.	0.470	0.200

are indispensable for protein synthesis (Christensen, 1990; McGivan and Pastor-Anglada, 1994). Among the amino acid transport systems described, system L is a major rout for providing cells with large neutral amino acids including branched or aromatic amino acids (Cornford *et al.*, 1992; Gomes and Soares-da-Silva, 1999). LAT1 is a system L amino acid transporter which transports a lot of essential amino acids. It is proposed to be at least one of the amino acids transporters essential for tumor cell growth (Yanagida *et al.*, 2001). High level of expression of LAT1 in tumor cells was indicated in tumor masses of various tissue origins as well as various tumor cell lines to support the high protein synthesis for cell growth and cell activation (Kanai *et al.*, 1998; Sang *et al.*, 1995; Wolf *et al.*, 1996). Since LAT1 is an amino acid transporter essential for tumor cell growth, one can expect that inhibition of LAT1 function may be a rational to anti-cancer therapy to suppress tumor growth (Kim *et al.*, 2004). BCH

is an amino acid-related compound which has been used as a selective inhibitor of system L (Christensen, 1990; Christensen *et al.*, 1969). Our previous studies have shown that BCH exert inhibitory effects on T24 cells through inhibition of LAT1 (Kim *et al.*, 2002). We confirmed this for T24 cells by showing that BCH in logarithmic phase of cell growth curve inhibits cell proliferation (Fig. 1).

Determining of gene expression profiles of T24 bladder carcinoma cells after BCH treatment is important for designing new anticancer drugs. It is possible to analyze the expression profiles of a large number of genes simultaneously using microarray. In this study, we utilized the high throughput gene chip, which contains 39,000 known genes, to determine the alternation of gene expression profiles of T24 bladder carcinoma cells exposed to BCH. Our results from cDNA microarray provided a complex cellular and molecular response to BCH treatment that likely to be mediated by a variety of regulatory pathways. We found that the molecular response to BCH in T24 bladder carcinoma cells involved inhibition or induction of genes that are related to biochemical, biological and regulatory processes in the cells. These genes have specific functions in cell proliferation, DNA metabolism, enzyme reaction, RNA binding, signal transduction, transcription, and transport. General tendency was up-regulation of these genes at 3 h and down-regulation at 12 h after BCH treatment (Fig. 2 and 3). These results suggest that inhibition of LAT1 by BCH may modulate the expression of first-response genes at an earlier stage (3 h), and in turn, alter the expression of intracellular second messenger molecules, resulting in cell adaptation for survival. At later stage (12 h), cellular response to BCH may involve modulation of gene expression for cell growth inhibition. For example up regulation of genes that are involved in cell proliferation at 3 h provide cellular pathways for survival and adaptation whereas down regulation of this group of genes at 12 h inhibit cell growth. Expression of interleukin 1 that stimulates proliferation (Beales, 2002; Kaden *et al.*, 2003; Olman *et al.*, 2002), significantly increased after 3 h and expression of deoxyhypusine synthase that causes growth in mammalian cells (Chen *et al.*, 1996; Park *et al.*, 1994; Shi *et al.*, 1996) decreased after 12 h, suggesting that BCH may inhibit cell growth through regulation of the expression of these important genes related to cell proliferation.

In signal transduction group, up regulation of Sorting nexin 11, GRO2 oncogene, Epiregulin, Adenosine A1 receptor, Inhibin alpha and down regulation of KIAA1075 protein were observed at 3 h whereas down regulation of Regulator of G-protein signalling 4, Integrin alpha 9, Endothelin receptor type B, ADP-ribosylation factor related protein 1, LIM domain only 7, Enigma (LIM domain protein) and up regulation of Hypothetical protein and Opsin 3 (encephalopsin, panopsin) were observed at 12 h, suggesting that cell signal transduction pathways is important for cell growth inhibition *via* LAT1 inhibitor.

In summary, we have analyzed the gene expression profiles of T24 bladder carcinoma cells exposed to BCH. BCH altered the expressions of many genes that are related to the control of cell proliferation, DNA metabolism, enzyme reaction, RNA binding, signal transduction, transcription, and transport. The gene expression profiles revealed novel molecular mechanisms by which BCH exerts its inhibitory effects on bladder carcinoma. BCH-induced regulation of these genes may be exploited for mechanism-based therapeutic strategies and new drugs development for bladder carcinoma. However, further in-depth studies are required to investigate the effects of BCH on the regulation of important cellular molecules at the protein levels to examine the effects of BCH on cellular pathways.

REFERENCES

Beales, I. L., Effect of Interlukin-1â on proliferation of gastric epithelial cells in culture. *BMC Gastroenterol.*, 2, 7 (2002).

Chen, Z. P., Yan, Y. P., Ding, Q. J., Knapp, S., Potenza, J. A., Schugar, H. J., and Chen, K. Y., Effects of inhibitors of deoxyhypusine synthase on the differentiation of mouse neuroblastoma and erythroleukemia cells. *Cancer lett.*, 105, 233-239 (1996).

Christensen, H. N., Role of amino acid transport and countertransport in nutrition and metabolism. *Physiol. Rev.*, 70, 43-77 (1990).

Christensen, H. N., Handlogten, M. E., Lam, I., Tager, H. S., and Zand, R., A bicyclic amino acid to improve discriminations among transport systems. *J. Biol. Chem.*, 244, 1510–1520 (1969).

Cornford, E. M., Young, D., Paxton, J. W., Finlay, G. J., Wilson, W. R., and Pardridge, W. M., Melphalan penetration of the blood-brain barrier via the neutral amino acid transporter in tumor-bearing brain. *Cancer Res.*, 52, 138-143 (1992).

Gomes, P. and Soares-da-Silva, P., L-DOPA transport properties in an immortalised cell line of rat capillary cerebral endothelial cells, RBE 4. *Brain Res.*, 829, 143-150 (1999).

Kaden, J. J., Dempfle, C. E., Grobholz, R., Tran, H. T., Kilic, R., Sarikoc, A., Brueckmann, M., Vahl, C., Hagl, S., Haase, K. K., and Borggrefe, M., Interleukin-1 beta promotes matrix metalloproteinase expression and cell proliferation in calcific aortic valve stenosis. *Atherosclerosis*, 170, 205-211 (2003).

Kanai, Y. and Endou, H., Heterodimeric amino acid transporters: molecular biology and pathological and pharmacological relevance. *Curr. Drug Metab.*, 2, 339-354 (2001).

Kanai, Y., Segawa, H., Miyamoto, K., Uchino, H., Takeda, E., and Endou, H., Expression cloning and characterization of a transporter for large neutral amino acids activated by the

heavy chain of 4F2 antigen (CD98). *J. Biol. Chem.*, 273, 23629–23632 (1998).

Kanno, J., Aisaki, K. I., Igarashi, K., Nakatsu, N., Ono, A., Kodama, Y., and Nagao, T., "Per cell" normalization method for mRNA measurement by quantitative PCR and microarrays. *BMC Genomics*, 7, 64 (2006).

Kim, D. K., Kanai, Y., Choi, H. W., Tangtrongsup, S., Chairoungdua, A., Babu, E., Tachampa, K., Anzai, N., Iribe, Y., and Endou, H., Characterization of the system L amino acid transporter in T24 human bladder carcinoma cells. *Biochim. Biophys. Acta*, 1565, 112-121 (2002).

Kim, D. K., Kim, I. J., Hwang, S., Kook, J. H., Lee, M. C., Shin, B. A., Bae, C. S., Yoon, J. H., Ahn, S. G., Kim, S. A., Kanai, Y., Endou, H., and Kim, J. K., System L-amino acid transporters are differently expressed in rat astrocyte and C6 glioma cells. *Neurosci. Res.*, 50, 437-446 (2004).

Li, Y. and Sarkar, F. H., Gene expression profiles of genistein-treated PC3 prostate cancer cells. *J. Nutr.*, 132, 3623-3631 (2002).

Macgregor, P. F. and Squire, J. A., Application of microarrays to the analysis of gene expression in cancer. *Clin. Chem.*, 48, 1170-1177 (2002).

McGivan, J. D. and Pastor-Anglada, M., Regulatory and molecular aspects of mammalian amino acid transport. *Biochem. J.*, 299, 321-334 (1994).

Olman, M. A., White, K. E., Ware, L. B., Cross, M. T., Zhu, S., and Matthay, M. A., Microarray analysis indicates that pulmonary edema fluid from patients with acute lung injury mediates inflammation, mitogen gene expression, and fibroblast proliferation through bioactive interleukin-1. *Chest*, 121 Suppl 3, 69-70 (2002).

Oxender, D. L. and Christensen, H. N., Evidence for two types of mediation of neutral amino acid transport in Ehrlich cells. *Nature*, 197, 765-767 (1963).

Park, M. H., Wolff, E. C., Lee, Y. B., and Folk, J. E., Antiproliferative effects of inhibitors of deoxyhypusine synthase. Inhibition of growth of Chinese hamster ovary cells by guanyl diamines. *J. Biol. Chem.*, 269, 27827-27832 (1994).

Sang, J., Lim, Y. P., Panzia, M., Finch, P., and Thompson, N. L., TA1, a highly conserved oncofetal complementary DNA from rat hepatoma, encodes an integral membrane protein associated with liver development, carcinogenesis, and cell activation. *Cancer Res.*, 55, 1152-1159 (1995).

Shi, X. P., Yin, K. C., Ahern, J., Davis, L. J., Stern, A. M., and Waxman, L., Effects of N1-guanyl-1, 7-diaminoheptane, an inhibitor of deoxyhypusine synthase, on the growth of tumorigenic cell lines in culture. *Biochim. Biophys. Acta*, 1310, 119-126 (1996).

Wolf, D. A., Wang, S., Panzia, M. A., Bassily, N. H., and Thompson, N. L., Expression of a highly conserved oncofetal gene, TA1/E16, in human colon carcinoma and other primary cancers: homology to Schistosoma mansoni amino acid permease and Caenorhabditis elegans gene products. *Cancer Res.*, 56, 5012-5022 (1996).

Yanagida, O., Kanai, Y., Chairoungdua, A., Kim, D. K., Segawa, H., Nii, T., Cha, S. H., Matsuo, H., Fukushima, J., Fukasawa, Y., Tani, Y., Taketani, Y., Uchino, H., Kim, J. Y., Inatomi, J., Okayasu, I., Miyamoto, K., Takeda, E., Goya, T., and Endou, H., Human L-type amino acid transporter 1 (LAT1): characterization of function and expression in tumor cell lines. *Biochim. Biophys. Acta*, 1514, 291-302 (2001).

ELSEVIER

Experimental Hematology

Experimental Hematology 35 (2007) 1190–1200

Glycolytic inhibition by mutation of pyruvate kinase gene increases oxidative stress and causes apoptosis of a pyruvate kinase deficient cell line

Ken-ichi Aisaki[a], Shin Aizawa[b], Hisaichi Fujii[c], Jun Kanno[a], and Hitoshi Kanno[c,d,e]

[a]*Cellular and Molecular Toxicology Division, National Institute of Health and Sciences, Tokyo, Japan;* [b]*Department of Anatomy, Nihon University School of Medicine, Tokyo, Japan;* [c]*Department of Transfusion Medicine and Cell Processing;* [d]*Institute of Medical Genetics; and* [e]*Division of Genomic Medicine, Department of Advanced Biomedical Engineering and Science, Graduate School of Medicine, Tokyo Women's Medical University, Tokyo, Japan*

(Received 13 November 2006; revised 8 May 2007; accepted 9 May 2007)

Objective. **SLC3 is a Friend erythroleukemic cell line established from the *Pk-1*^{slc} mouse, a mouse model of red blood cell type-pyruvate kinase (R-PK) deficiency. This study was aimed to elucidate the mechanisms attributing to apoptosis induced by R-PK deficiency.**

Materials and Methods. **SLC3 and a control Friend cell line, CBA2, were cultured in a condition of glucose deprivation or supplementation with 2-deoxyglucose, and apoptosis was detected by annexin V. We established two stable transfectants of SLC3 cells with human R-PK cDNA, and examined the effect of R-PK on an apoptotic feature by cell cycle analysis. Intracellular oxidation was measured with 2′,7′-dichlorofluorescin diacetate. DNA microarray analysis was performed to examine gene-expression profiles between the two transfectants and parental SLC3.**

Results. **SLC3 was more susceptible than CBA2 to apoptosis induced by glycolytic inhibition. The forced expression of R-PK significantly decreased cells at the sub G_0/G_1 stage in an expression-level dependent manner. Microarray analysis showed that proapoptotic genes, such as *Bad*, *Bnip3*, and *Bnip3l*, were downregulated in the transfectants. In addition, peroxiredoxin 1 (*Prdx1*) and other antioxidant genes, such as *Cat*, *Txnrd1*, and *Glrx1* were also downregulated. A significant decrease of dichlorofluorescein fluorescence was observed by R-PK expression. Preincubation with a glutathione precursor showed a significant decrease of apoptosis.**

Conclusion. **These results indicated that glycolytic inhibition by R-PK gene mutation augmented oxidative stress in the Friend erythroleukemia cell, leading to activation of hypoxia-inducible factor-1 as well as downstream proapoptotic gene expression. Thus, R-PK plays an important role as an antioxidant during erythroid differentiation.** © **2007 ISEH - Society for Hematology and Stem Cells. Published by Elsevier Inc.**

Glycolysis is an essential metabolic pathway in all organisms. Pyruvate kinase (PK) is a key glycolytic enzyme, and has four isoenzymes in mammals, designated M_1, M_2, L (liver), and R (red blood cell). In humans, these isozymes are encoded by two structural genes, *PKM* and *PKLR*, respectively [1]. M_2-PK is the only isozyme that is active in early fetal tissues and also almost ubiquitously expressed in adult tissues, including hematopoietic stem cells, progenitors, leukocytes, and platelets. Red blood cell type-pyruvate kinase (R-PK) becomes a major isozyme during erythroid differentiation/maturation [2,3], and in mature red blood cells (RBCs), R-PK is the only detectable PK isozyme. Deficiency of R-PK causes shortened RBC survival, resulting in hemolytic anemia. In humans, PK deficiency is the most prevalent glycolytic enzyme defect, which is responsible for hereditary hemolytic anemia [4,5].

We have previously established SLC3 [6], a line of Friend erythroleukemic cells from the *Pk-1*^{slc} mouse [7], which has chronic hemolytic anemia with marked splenomegaly due to a missense mutation of the murine *Pklr* gene [8]. SLC3 showed spontaneous apoptosis during routine passage and in vitro erythroid differentiation by butyrate exacerbated apoptosis of SLC3 [6]. Recently, we examined the spleen of a subject with severe PK deficiency [9], and discovered enhanced extramedullary hematopoiesis as well as apoptotic erythroid cells. Enhanced apoptosis

Offprint requests to: Hitoshi Kanno, M.D. Ph.D., Department of Transfusion Medicine and Cell Processing, Tokyo Women's Medical University, Tokyo 162-8666, Japan.

0301-472X/07 $–see front matter.
doi: 10.1016/j.exphem.2007.05.005

was also identified in TER119-positive erythroid cells isolated from *Pk-1*^{slc} mice [10]. These results provide evidence that the metabolic disturbances in PK deficiency affect not only the survival of RBCs but also the maturation of erythroid progenitors, which results in apoptosis.

In this study, we examined whether Friend erythroleukemic cell lines showed apoptosis when glycolysis was inhibited. To evaluate whether overexpression of the normal R-PK gene ameliorated apoptosis, we established stable transfectants of SLC3 and compared their apoptotic characteristics and transcriptional profiles with parental SLC3. We present here several pieces of evidence, revealing the biological significance of R-PK to suppress oxidative stress during erythroid differentiation.

Materials and methods

Cell culture and flow cytometric analysis

Friend erythroleukemic cell lines SLC3 and CBA2 have been described previously [6]. Both cell lines are maintained in Iscove's modified Dulbecco's medium (Invitrogen, Carlsbad, CA, USA) supplemented with 10% heat-inactivated fetal calf serum, 20 μM 2-mercaptoethanol, and a mixture of penicillin-streptomycin (Sigma-Aldrich, St Louis, MO, USA).

To evaluate the adverse effects of glycolytic inhibition, cells were cultured in either glucose-free RPMI-1640 (Invitrogen) or RPMI-1640 with 2-deoxyglucose (2-DG) at final concentrations of 0.1, 1, and 10 mM. Iscove's modified Dulbecco's medium containing 110 mg/L sodium pyruvate, and RPMI-1640 containing no pyruvate.

Flow cytometric analysis was performed by EPICS XL and analyzed with software, EXPO32 ADC (Beckman-Coulter, Fullerton, CA, USA). Annexin V-Alexa568 and rhodamine 123 were obtained from Roche Diagnostics (Basel, Switzerland) and Sigma, respectively. To examine the effect of N-acetyl-L-cysteine upon apoptosis, we preincubated cells in RPMI-1640 supplemented with 10 mM N-acetyl-L-cysteine for 12 hours, followed by 12- to 24-hour incubation with RPMI-1640.

Establishment of stable transfectants expressing normal R-PK in SLC3 cells

We constructed a human R-PK cDNA expression plasmid vector in erythroid cells. A 1.7-kb fragment covering the entire coding region of human R-PK cDNA [11] was introduced into *Kpn*I-*Eco*RV sites of pcDNA3.1 (Invitrogen). Plasmid DNA was purified with an EndoFree Maxi DNA purification kit (Qiagen, Hilden, Germany). Transfection was done with Effectene Transfection Reagent (Qiagen) as indicated by the manufacturer. Transfected cells were selected using G418 (400 μg/mL).

RT-PCR, Western blotting, and enzyme assay

Total cellular RNA was extracted with an RNeasy purification kit (Qiagen), and 2 μg RNA was reverse-transcribed (RT) at 42°C for 90 minutes with 50 pmole oligo (dT)17 primer, 0.5 U/μL cloned RNase inhibitor (Takara Bio, Shiga, Japan), 10 mM dithiothreitol, 1 mM deoxyribonucleoside triphosphate, and 50 U Expand Reverse Transcriptase (Roche Diagnostics). Aliquots (1/10) were subjected to PCR using primer pairs specifically amplified with human and murine R-PK cDNA, hRPK-F (5′-TGGCCCAGC CTACCCTTGTA-3′)/hRPK-R (5′-CTTAAAGGTGGGGCTTTG GA-3′) and mRPK-F (5′-GCAGATGATGTGGACCGAAG-3′)/ mRPK-R (5′-CTAGATGGCAGATGTGGGACTA-3′), respectively. The reaction mixtures were subjected to 40 cycles of amplification consisting of 94°C for 20 seconds, 60°C for 10 seconds, and 72°C for 10 seconds for hRPK and 94°C for 20 seconds, 60°C for 20 seconds, and 72°C for 20 seconds for mRPK in a GeneAmp PCR system 2400 (Roche Diagnostics, Switzerland), and separated using 2% agarose gel electrophoresis.

For Western blot analysis, cells were harvested, followed by washing with phosphate-buffered saline twice. Following three-times freezing and thawing in extraction buffer (10 mM Tris/ HCl, pH 8.0, 10 mM $MgCl_2$, 0.003% 2-mercaptoethanol, 0.02 mM ethylenediamine tetraacetic acid), cell extracts were obtained for Western blot analysis. Protein assays were performed by the method of Bradford using a commercial kit (Bio-Rad Laboratories, Hercules, CA, USA).Western blot analysis was conducted using anti-rat L-PK (kindly provided Tamio Noguchi, Nagoya University) and ECL advance Western Blotting Detection Kit (Amersham Biosciences, Buckinghamshire, UK).

PK and lactate dehydrogenase (LDH) activity was measured, as described [12].

Microarray analysis

To prepare high-quality total cellular RNA for the GeneChip assay, RNA was extracted with modified protocols using the TRIzol LS (Invitrogen) and RNeasy purification kit (Qiagen). Briefly, cells were harvested with no washing step, and immediately homogenized with the RLT buffer. The lysate was then mixed with 3 volumes of the TRIzol LS. After a 10-minute incubation at room temperature, the sample solution was mixed with an equal volume of chloroform. The sample was centrifuged at 10,000*g* for 15 minutes at 4°C, and then the upper aqueous phase was transferred to a fresh tube. After mixing with an equal volume of 70% ethanol, the sample was incubated for 10 minutes at room temperature. Without any flash step, the sample solution was transferred to the RNeasy column, and then processed by the manufacturer recommended protocol.

To normalize the variation in data based on the cell count, we used *Bacillus subtilis* RNA for an external standard signal, which was added to the cell lysate in proportion to the sample's DNA contents [13]. Ten microliters of cell lysate was provided for DNA quantification using Picogreen (Invitrogen). GeneChip (Affymetrix, Santa Clara, CA, USA) analysis was carried out according to the Affymetrix-recommended protocols. Processed RNA was hybridized to the Affymetrix Murine Genome 430A arrays (22960 probe sets). Signal values were calculated from scanned images by the Affymetrix Microarray Operation System (GCOS). The cell sample was pooled from six culture dishes at each condition and one GeneChip was used per one pooled sample.

Data analysis

Data were normalized by an original program (SCal), which processes data in proportional conversion based on the DNA content of each biosample [13]. This DNA content-based normalization method improves the measurement accuracy of GeneChip. For example, a series of samples was measured by quantitative PCR and Affymetrix GeneChip microarrays using this method, and the results showed up to 90% concordance [13].

To identify differentially expressed genes, we used an empirical threshold calculated by an original algorithm (Fx). The Fx threshold is based on the signal intensity level and is calculated as follows: $Y = X \cdot (1 + RC^{(w-\log X)})$ and $Y = X \cdot (1 + C^{(w-\log X)})^{-1}$ (Fx1 and Fx2 respectively; C and w are constant parameters reflecting actual measurement data by GeneChip hybridized with the standard sample). C and w were set to 3.0 and 2.5, respectively, which was equivalent to $p < 0.02$. In the scatter plot, the spots above the Fx1 line were evaluated as upregulated, and the spots below the Fx2 line were evaluated as downregulated.

Results

SLC3 is more susceptible than the control to apoptosis due to glycolytic inactivation

Figure 1 shows flow cytometric analysis using annexin V (horizontal axis) and rhodamine 123 (vertical axis) to examine the effects of glycolysis inhibition on Friend leukemic cells with or without R-PK mutation. SLC3 showed spontaneous apoptosis during routine passage, and apoptosis preceded mitochondrial dysfunction in the R-PK–deficient erythroleukemia cells as reported previously [6]. The result showed that a part of apoptotic cells kept similar mitochondrial transmembrane potentials and that SLC3 were much more susceptible to glucose deprivation as well as 2-DG.

Overexpression of wild-type R-PK decreases apoptosis of SLC3

In order to evaluate how wild-type R-PK rescues apoptotic phenotypes, we established two stable transfectants of SLC3 with overexpression of the human R-PK cDNA. Figure 2 shows RT-PCR and Western blot analysis of a parental SLC3 and SLC3-hRPK.Hi (hRPK.Hi) and SLC3-hRPK.Lo (hRPK.Lo). As shown in Figure 2A, the expression level of the transgene was higher in hRPK.Hi than hRPK.Lo. Overexpression of human R-PK suppressed endogenous R-PK expression as observed in the lane of hRPK.Hi.

Enzymatic analysis of transfectants revealed that PK activities of hRPK.Lo and Hi were 17.2 and 24.2 IU/mg protein, respectively. The PK activity of hRPK.Hi was almost comparable to parental SLC3, 23.5 IU/mg protein. It should be noted that endogenous LDH activity was decreased by transgene expression, leading to a PK/LDH ratio increase from 0.4 (SLC3) to 0.48 (hRPK.Lo) and 0.6 (hRPK.Hi).

We evaluated apoptosis of the two transfectants by cell cycle analysis. Figure 2C shows that the expression of wild-type R-PK decreased the number of cells at the sub-G_0/G_1 stage. While hRPK.Lo showed almost the same number of sub-G_0/G_1 cells (55.5%) as SLC3 (57.4%), only 19.3% of hRPK.Hi were arrested at the sub G_1-stage. Because apoptotic cells were rescued from apoptosis in an R-PK expression level-dependent manner, it is most likely that R-PK activity is required to suppress apoptosis of erythroid cells.

Microarray analysis elucidates the differential expression of genes involved in reactive oxygen species removal, cell cycle, and apoptosis

Gene expression profiles between the two transfectants and the parental SLC3 cell line were analyzed by DNA microarray analysis. After exchanging culture medium, SLC3, hRPK.Lo, and Hi were sampled at 24 and 67 hours, which were the phase of reentry into cell cycling and of subconfluence, respectively. Transgene expression upregulated only about 2% (469 probe sets) of genes, whereas approximately 25% (5754 probe sets) of genes were downregulated both in hRPK.Hi and hRPK.Lo at 24 and/or 67hours. As shown in Figure 3B, major categories of the downregulated genes involved the cell cycle, development, and apoptosis. Proapoptotic genes including *Bad*, *Bnip3*, and *Bnip3l*, as well as *Casp 2, 6, 7,* and *8* were downregulated (Figs. 3A and 4).

Genes of key glycolytic enzymes such as hexokinase-2 (*Hk2*), phosphofructokinase (*Pfkl*), phosphoglycerate kinase (*Pgkl*), and PK (*Pklr*) were downregulated, and expression levels were characteristically decreased after 67 hours of transfection, suggesting that suppression requires protein synthesis.

It should be noted that genes for antioxidant protein, such as peroxiredoxin 1 (*Prdx1*) and related genes, such as catalase (*Cat*), thioredoxin reductase 1 (*Txnrd1*), and glutaredoxin 1 (*Glrx1*), which have a role in the modulation of oxidative stress, are also downregulated. As for *Prdx2*, expression change by the transgene was not evident. Intracellular reactive oxygen species (ROS) are known to cause DNA damage, inducing the expression of DNA repair genes. In this experiment, expressions of genes involved in DNA repair were decreased, including *Brca1*, *Brca2*, and *Rad51*.

PK gene mutation and glycolytic inhibition by 2-DG augment intracellular ROS

We examined intracellular ROS in SLC cells and control CBA2 cells by 2′,7′-dichlorofluorescin-diacetate (DCFH-DA), an indicator of the intracellular formation of hydrogen peroxide and free radicals. Nonfluorescent DCFH-DA turns into DCFH (2′,7′-dichlorofluorescin) in the presence of hydrogen peroxide, and then DCFH is quickly photo-oxidized to fluorescent DCF (2′,7′-dichlorofluorescein).

Figure 5A shows that SLC3 is hypersensitive to a glycolytic inhibitor, 2-DG, producing intracellular DCF by adding 1 mM 2-DG. In contrast, control CBA2 cells do not produce DCF even at 10 mM 2-DG for 30 minutes.

Reduced glutathione (GSH) is an important antioxidant in erythrocytes. GSH is produced by a two-step enzymatic reaction involving γ-glutamylcystein synthetase and glutathione synthetase (GSH-S). Apoptosis induced either by the glycolytic gene mutation (SLC3) or the glycolytic inhibitor (CBA with 2-DG) was suppressed by preincubation with the glutathione precursor, NAC (Fig. 5B). Finally, the